




CHEMICAL PRESERVATION OF TAIL FEATHERS FROM *ANCHIORNIS HUXLEYI*, A THEROPOD DINOSAUR FROM THE TIAOJISHAN FORMATION (UPPER JURASSIC, CHINA)

by AUDE CINCOTTA¹ , THANH THUY NGUYEN TU², JULIEN L. COLAUX³, GUY TERWAGNE⁴, SYLVIE DERENNE², PASCAL GODEFROIT⁵, ROBERT CARLEER⁶, CHRISTELLE ANQUETIL² and JOHAN YANS⁷

¹School of Biological, Earth & Environmental Sciences, University College Cork, Distillery Fields, North Mall, Cork, T23 N73K, Ireland; aude.cincotta@ucc.ie

²CNRS, EPHE, PSL, Sorbonne Université, UMR 7619 Metis, 4 place Jussieu, 75252, Paris Cedex 05, France

³Synthesis, Irradiation & Analysis of Materials (SIAM), Department of Physics, University of Namur, 61 rue de Bruxelles, 5000, Namur, Belgium

⁴Laboratoire d'Analyses par Réactions Nucléaires (LARN), Department of Physics, University of Namur, 61 rue de Bruxelles, 5000, Namur, Belgium

⁵Operational Directorate 'Earth & History of Life', Royal Belgian Institute of Natural Sciences, 29 rue Vautier, 1000, Brussels, Belgium

⁶Applied & Analytical Chemistry, Institute for Material Research, University of Hasselt, Campus Diepenbeek, Agoralaan Building D, 3590, Diepenbeek, Belgium

⁷Institute of Life, Earth & Environment, University of Namur, 61 rue de Bruxelles, 5000, Namur, Belgium

Typescript received 17 October 2018; accepted in revised form 16 April 2020

Abstract: A panel of geochemical techniques is used here to investigate the taphonomy of fossil feathers preserved in association with the skeleton of the Jurassic theropod *Anchiornis huxleyi*. Extant feathers were analysed in parallel to test whether the soft tissues morphologically preserved in the fossil also exhibit a high degree of chemical preservation. Scanning electron microscopy (SEM) and energy dispersive spectroscopy (EDS) indicate that clays and iron oxide pseudomorphs occur in the surrounding sediment and also reveal the preservation of melanosome-like microbodies in the fossil. Carbon gradient along a depth profile and co-occurrence of carbon and sulphur are shown in the fossil by elastic backscattering (EBS) and particle-induced x-ray emission (PIXE), which are promising techniques for the elemental analysis of fossil soft tissues. The molecular composition of modern and fossil soft tissues was assessed from micro-attenuated total reflectance fourier transform

infrared spectroscopy (micro-ATR FTIR), solid-state ¹³C nuclear magnetic resonance (CP-MAS ¹³C NMR) and pyrolysis gas chromatography mass spectrometry in the presence of TMAH (TMAH-Py-GC-MS). Results indicate that the proteinaceous material that comprises the modern feathers is not present in the fossil feathers. The fossil feathers and the embedding sediment exhibit a highly aliphatic character. However, substantial differences exist between these samples, revealing that the organic matter of the fossil feathers is, at least partially, derived from original constituents of the feathers. Our results suggest that, despite the morphological preservation of *Anchiornis* feathers, original proteins, that is keratin, were probably not preserved in the 160-myr-old feathers.

Key words: *Anchiornis*, fossil feather, taphonomy, soft tissue preservation, dinosaur.

PRESERVATION of soft parts (non-mineralized tissues) in animals is relatively rare when considering the whole geological record. Soft parts of organisms are usually lost during the diverse degradation processes occurring during fossilization. Their constitutive labile organic compounds are usually too fragile to be preserved, compared to the 'hard' (biomineralized) parts, which are generally better preserved. However, some important fossil-bearing sites yield not only exquisitely preserved skeletons but also remains of soft tissues, such as skin, scales, hair or

feathers (Allison & Briggs 1993; Zhu *et al.* 2005; Pan *et al.* 2013). Feathers, the epidermal appendages that form the external covering of modern birds, have been discovered preserved in close association with fossils of theropod dinosaurs in Konservat-Lagerstätten (localities that are characterized by the unusual quality of the fossils) from the Upper Jurassic and Lower Cretaceous of China (Xu *et al.* 1999, 2009, 2012; Hu *et al.* 2009; Godefroit *et al.* 2013; Chu *et al.* 2016) and the Upper Jurassic of Germany (Rauhut *et al.* 2012). During the last 20 years,

Liaoning Province, in north-eastern China, has yielded well-preserved vertebrate fossils with soft parts (Benton *et al.* 2008; Kellner *et al.* 2010; Li *et al.* 2012). The most striking discoveries were exquisitely well-preserved feathered theropod dinosaurs, evidencing their relationship with modern birds. Since the discovery of the Early Cretaceous *Sinosauropteryx prima* (Ji & Ji 1996), many other feathered specimens have been found (Hu *et al.* 2009; Li *et al.* 2012; Xu *et al.* 2012, 2015). In the same way, the discovery of one of the most primitive birds, *Archaeopteryx lithographica*, associated with well-preserved feathers, constitutes a gigantic step in the comprehension of bird, and feather, evolution (Christiansen & Bonde 2004). Interestingly, elongate filaments interpreted as primitive feathers were observed in ornithischian (non-theropod) dinosaurs (Mayr *et al.* 2002; Zheng *et al.* 2009). Recently, both ‘feather-like’ structures and scales were discovered together with remains of the middle Jurassic neornithischian *Kulindadromeus zabaikalicus* collected from volcanoclastic deposits in Siberia (Godefroit *et al.* 2014, 2020; Cincotta *et al.* 2019). Recently, a small theropod dinosaur, the scansoriopterygid *Amblopteryx longibrachium* (Wang *et al.* 2019) from the Upper Jurassic of China, was described with membranous wings instead of feathered ones. This wing configuration was probably lost during evolution in favour of the feathered wing configuration that occurs in modern birds.

In a recent study, Zhao *et al.* (2020) observed the structure of experimentally matured feathers and reported the fusion of barbs in the matured feathers. This result has implications in terms of feather taphonomy and evolution, for the absence of barbs in fossil feathers could be, according to the authors, due to their fusion during diagenesis rather than their true absence in the specimen. The addition of chemical analyses to this study would have probably allowed a better understanding of how maturation affects the preservation of biomolecules in feathers.

Fossil feathers show a wide range of degrees of preservation (Schweitzer 2011; Xing *et al.* 2016). The study of these diversely preserved structures is crucial for a better understanding of the taphonomic processes leading to their preservation. In most cases, feathers and other types of preserved soft-tissues were deposited in calm, low-energy environments (Kellner & de Almeida Campos 2002). They are found in diverse environmental settings such as shallow-marine (Barthel 1964; Heimhofer & Martill 2007; Martill & Heimhofer 2007), lacustrine (Harms 2002; Zhou *et al.* 2010; Sullivan *et al.* 2014), or terrestrial (Manning *et al.* 2013). Different modes of preservation occur for ancient soft tissues: carbonaceous films (Li *et al.* 2010; Lindgren *et al.* 2015), phosphate (Allison & Briggs 1993; Briggs *et al.* 1993), pyrite (Briggs *et al.* 1991; Leng & Yang 2003; Farrell *et al.* 2013), clay minerals (Gabbott

et al. 2001; Martin *et al.* 2004), aluminosilicates (Butterfield *et al.* 2007) or a combination of these (Wilby *et al.* 1996).

Feathers are epidermal appendages mainly composed of keratin (Lucas & Stettenheim 1972), which is present as two secondary structures, alpha-helices and beta-sheets, corresponding to alpha and beta-keratin, respectively (Fraser & MacRae 2012). Alpha-keratin plays a hydrophobic role in avoiding water loss, whereas beta-keratin increases skin hardness (Gregg & Rogers 1986; Fraser & Parry 1996). According to Lucas & Stettenheim (1972), the amino acid content of keratin in modern bird feathers is rather homogenous in identical parts of a feather (e.g. in the rachis of feathers belonging to the same species), although it varies from one species to another. Nonetheless, feather keratin always comprises high amounts of serine, glycine, proline, and lower quantities of valine, leucine, alanine and cysteine (O'Donnell & Inglis 1974; Arai *et al.* 1983, 1986; Gregg & Rogers 1986; Murphy *et al.* 1990; Staroń *et al.* 2011; Saravanan & Dhurai 2012).

The potential of keratin to resist diagenetic processes is still poorly known. Saitta *et al.* (2017) performed decay and maturation experiments of various keratinous structures which suggested that feather keratin would not survive diagenesis. Although the ultrastructure of feather keratin, that is fibrils, can be preserved (Lindgren *et al.* 2015), there is no direct evidence for the preservation of its proteinaceous compounds. Several immunohistological studies have suggested that keratin could be preserved (Schweitzer *et al.* 1999; Moyer *et al.* 2016; Pan *et al.* 2016), although this method remains highly controversial. By contrast, melanin (the natural pigment present in a variety of soft tissues including hair, skin and feathers) is considered to be more resistant to degradation and fossilization processes. Melanin has been unequivocally identified in various types of fossil tissues, such as fish eyes (Lindgren *et al.* 2012), bird feathers (Colleary *et al.* 2015), non-avian dinosaur feathers (Lindgren *et al.* 2015), mammal hair (Colleary *et al.* 2015) and frog skin (McNamara *et al.* 2016).

Here, we investigate the ultrastructure and chemical composition of fossil feathers of a theropod dinosaur, *Anchiornis huxleyi* (YFGP-T5199), collected from Upper Jurassic deposits of the Tiaojishan Formation (Liaoning Province, China). Previous study of the same specimen focused on the identification of pigment remains (eumelanin), and evidenced the preservation of melanosomes in the feathers (Lindgren *et al.* 2015). We report new and complementary geochemical information about the preservation of macromolecular compounds in the fossil feathers using a range of analytical tools. The surrounding sediment and modern feathers were analysed in parallel to ascribe pristine constituents.

Scanning electron microscopy (SEM) and energy dispersive x-ray spectroscopy (EDS) were used to identify and characterize the elemental composition of preserved pigment organelles and the sedimentary matrix. X-ray diffraction (XRD) was used to analyse the mineralogical composition of the samples in an attempt to understand the role of sediment mineralogy in the preservation of soft tissues. Ion beam analysis (IBA), is recognized as a promising archaeometric tool (Jeynes & Colaux 2016) and has recently been successfully applied to human bone analyses (Beck 2014). In this work, particle-induced x-ray emission (PIXE) and elastic backscattering spectrometry (EBS) were used for the first time on fossil soft tissues to get insights into the heavy (PIXE) and light (EBS) in-depth elemental composition of the samples. This approach is innovative in the study of organic materials. Organic geochemistry techniques, micro-attenuated total reflectance Fourier transform infrared spectroscopy (micro-ATR FTIR), ^{13}C -nuclear magnetic resonance (NMR) and pyrolysis gas chromatography mass spectrometry in the presence of TMAH (TMAH-Py-GC-MS) were applied to characterize the functional groups and other biomolecular components present in the studied samples. To our knowledge, the detailed chemical characterization by ^{13}C NMR and Py-GC-MS of fossil feathers from a non-avian dinosaur has not been done elsewhere.

MATERIAL AND METHOD

Specimen information

The studied specimen, *Anchiornis huxleyi* (YFGP- T5199) (Fig. 1), is a basal Avialan (the description of the specimen is available in Lindgren *et al.* 2015, SI, pp 18–23) that was collected from the Tiaojishan Formation in the Yaolugou locality (Liaoning Province, China), and belongs to the Yizhou Fossil and Geology Park in Liaoning. The Tiaojishan Formation consists of hundreds of metres of alternating sedimentary and volcanic beds (Yuan *et al.* 2005; Yang *et al.* 2006; Liu *et al.* 2012). Absolute dating on a laterally equivalent formation (the Lanqi Formation) indicates an age ranging between 165.0 ± 1.2 and 153.0 ± 2.0 Ma (Zhang *et al.* 2008; Chang *et al.* 2009), which spans the Callovian–Kimmeridgian interval (Middle–Late Jurassic; Gradstein *et al.* 2012). YFGP- T5199 is embedded in thinly laminated carbonate sediments, corresponding to alternation of very thin marl and thicker clay laminae. These sediments were deposited in the context of a lake affected by episodic volcanic eruptions (Nan *et al.* 2012). Recent U–Pb radiochronological analyses on zircons from the Jianchang locality indicate that the Yanliao Biota, that includes *Anchiornis* as well as pterosaurs and eutherian mammals,

is Oxfordian in age (Chu *et al.* 2016). The plumage of the specimen studied herein is morphologically preserved as dark brown residues around the skeleton, especially around the tail and the forelimbs, and on the skull.

Sample description

The studied samples consist of fossil feather fragments dissected from the posterior end of the tail (Fig. 1, the dark area in the white box, top right) of YFGP- T5199, as well as fragments of the host sediment (Fig. 1, the light area in the white box). To test for possible chemical contamination of the fossil feathers by sediment, the sediment samples were analysed using the same methodology as for the fossil feathers. Two types of sediment samples were studied: (1) ‘host’ sediment directly in contact with the feathers from the tail (light area in white box on Fig. 1); and (2) ‘remote’ sediment located >100 mm from the fossil on the same slab (yellow box, bottom left on Fig. 1).

Sample preparation

Two modern brown wing feathers of *Buteo buteo* (buzzard; Aves, Accipitriformes; RBINS collection number: A4011A01; Cincotta *et al.* 2020, fig. S1) were analysed for comparative purposes. Different parts of the feathers, rachis and barbs, were analysed with IBA. The modern feathers come from a specimen that had died naturally and was stored at -18°C at the Royal Belgian Institute of Natural Sciences prior to analysis.

Two types of sample were collected on the fossil specimen: millimetre-sized samples for SEM and EDS, as well as centimetre-sized samples for the other analytical approaches. We took a total of 12 millimetre-sized samples (Fig. 1) from different regions of the body of YFGP- T5199 with a sterile scalpel. The samples were mounted on double-sided carbon tape and sputter-coated with gold (BAL-TEC SCD 050). Centimetre-sized fragments of approximately 5 mm^2 and 2 mm thick, from fossil feathers (white box in Fig. 1) and sediment (yellow box in Fig. 1) were dissected with a sterile scalpel. Samples were cleaned with distilled water without any additional preparation prior to analysis.

Several points were analysed with IBA and micro-ATR FTIR on two centimetre-sized fragments containing both fossil feathers and their ‘host’ sediment, and one fragment of ‘remote’ sediment (Cincotta *et al.* 2020, figs S1B, S2). Other centimetric samples from the same region were collected for NMR and Py-GC-MS (white and yellow boxes on Fig. 1). These samples were crushed and lipids were extracted in order to: (1) eliminate potential

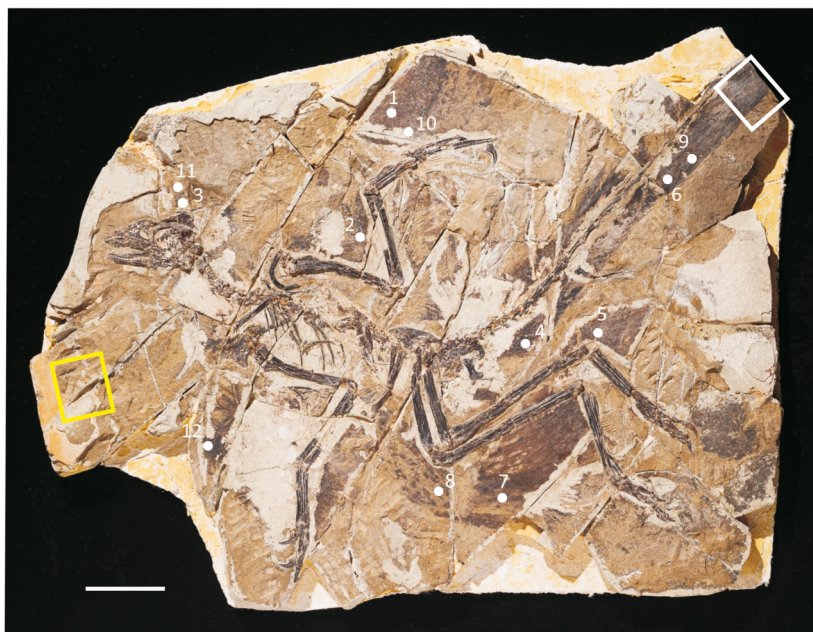


FIG. 1. *Anchiornis huxleyi* (YFGP-T5199). Photograph of the Jurassic feathered theropod with location of sampled areas. The white box (upper right) indicates locations of fossil feather and 'host' sediment sampling, while the yellow box (lower left) indicates location of 'remote' sediment sampling, for NMR, Py-GC-MS, and IBA analyses. White dots are samples used for SEM imaging and EDS. Scale bar represents 5 cm. Photograph by Thierry Hubin (RBINS). Colour online.

contaminants related to sample manipulation; and (2) concentrate macromolecular organic matter which mainly corresponds to proteins in modern feathers. Samples were ground to a fine homogeneous powder in an agate mortar. Lipid extraction involved three successive ultrasonifications (10 min) in 15 ml of dichloromethane/methanol (2:1, v/v), at room temperature and centrifugation at 1921 g (10 min). The supernatant was removed and the pellet was dried under nitrogen and stored in the dark at 5°C prior to analysis.

Analytical methods

Samples were imaged under low vacuum with an environmental QUANTA 200 (FEI) scanning electron microscope (at an acceleration voltage ranging from 20 to 30 kV and working distances of 8–15 mm). Subsequent semi-quantitative EDS analyses (single point and mapping) were performed using either an environmental QUANTA 200 (acceleration voltage of 30 kV and working distance of 10 mm) or a field-emission JEOL 7500F (acceleration voltage of 15 kV and a working distance of 8 mm).

XRD analyses were carried out on both bulk rock and clay mineral with a Philips diffractometer using Cu K α radiation. A tube voltage of 40 kV and a tube current of 30 mA were used. The goniometer scanned from 3° to 70°

(2 θ) for the bulk rock and from 3° to 30° (2 θ) for clay minerals. The clay minerals (<2 μ m fraction) were isolated by successive centrifuging after decarbonation of the crushed rock with 1N HCl. The preparation was mounted on glass slides and treated according to the three following protocols: (1) natural (air-dried); (2) ethylene-glycol solvation; and (3) heated at 490°C for 2 h. Clay minerals were identified according to the position of the (001), or (0001), series of basal reflections on the x-ray diffractograms.

EBS and PIXE measurements were performed using a 3 MeV proton (^1H) beam from the Tandatron linear accelerator ALTAIS (University of Namur). PIXE is highly sensitive to Na to U elements whereas EBS signals are enhanced for light elements (e.g. C, N and O) due to strong non-Rutherford cross-sections. These two integrative methods, together, can identify almost all elements of the periodic table. The beam spot size was reduced to 0.5 mm in diameter to minimize topographic effects. Backscattered particles were detected using two detectors mounted at scattering angles of 170° and 165°, whereas the emitted x-rays were collected with an ultra-LEGe (ultra low energy germanium) detector mounted at 135°. Angles are given relative to the incident beam direction. A selective filter (6 μ m of Al) was mounted in front of the ultra-LEGe detector to lower the strong Si signal and therefore enhance the rather weak S signal observed in the fossil feathers. The modern brown feathers were analysed at two different locations (barb and rachis; Cincotta

et al. 2020, figs S1, S2). Two locations were analysed in the fossil feathers. The ‘host’ sediment was analysed at three different locations (at 1.7, 3.2 and 4.8 mm away from the fossil) and the ‘remote’ sediment at one location (Cincotta *et al.* 2020, fig. S2). All the samples were analysed using the same experimental settings. A certified reference material (BCR-126A lead glass from NIST) was analysed to: (1) calibrate the detectors (both EBS and PIXE); and (2) estimate the accuracy of the PIXE measurements. The EBS spectra were analysed with DataFurnace software (Jeynes *et al.* 2003) together with the cross-sections generated by SigmaCalc (Gurbich 2016) to derive the depth profiles of the major elements (for C, see Cincotta *et al.* 2020, fig. S4). The integral of C, O and Si depth profiles (integration limits set to 0–25 000 TFU¹, or 0–3 μm considering a density of 2.65 g/cm³ for the sediment) yields the C, O and Si equivalent thicknesses given in TFU (details on the global uncertainty calculations can be found in Cincotta *et al.* 2020, table S1). The PIXE spectra were manipulated with GUPIX software (Campbell *et al.* 2010). The matrix composition to be used in GUPIX was determined by integrating the depth profiles of the main components observed by EBS (i.e. C, O and Si) on a given interval (0–100 000 TFU).

Micro-ATR FTIR was performed on modern and fossil feathers using a Bruker Vertex 70 FTIR spectrometer (University of Hasselt, Belgium) equipped with a Hyperion 2000 microscope and MCT detector. The infrared spectra were collected in the mid-IR range, from 4000 to 600 cm^{−1}, and 32 scans were acquired in attenuated total reflectance (ATR) mode (Ge-ATR crystal) with a resolution of 4 cm^{−1}. FTIR spectroscopy was used on a modern buzzard feather (dark regions), one sample of fossil feather from the tail of *A. huxleyi* and the surrounding sediment, to identify the presence or absence of functional groups in their molecular composition.

¹³C NMR is a spectroscopic method that documents the chemical environment of carbon in organic compounds. Solid state ¹³C NMR spectra of the lipid-free samples were obtained at 125 MHz (Bruker Avance 500 spectrometer) using a 4 mm zirconium rotor, with a cross-polarization (CP) sequence and magic angle spinning (MAS) at 14 kHz. CP-MAS ¹³C NMR spectra were acquired with contact time of 1 ms and recycle time of 1s (fossil and sediment) or 3s (modern feathers). The use of a single contact time does not allow precise quantification of the identified chemical functional groups. Each spectrum was the result of 6 000 (modern samples) to 400 000 (sediments) scans.

Curie point Py-GC-MS gives insight into the molecular composition of organic macromolecular materials through their thermal degradation into molecular building blocks that can be separated by gas chromatography (GC) and further identified by mass spectrometry (MS).

Tetramethylammonium hydroxide (TMAH) was used to enhance the thermal breakdown of macromolecules and induce *in situ* methylation of pyrolysis products, which, in turn, enhances their detection and identification in Py-GC-MS. The samples were mixed with an excess of TMAH (25 wt% in methanol) in a 1:1 (wt/wt) ratio before loading in ferromagnetic tubes with Curie temperature of 650°C. Masses of 2 mg were used for the modern samples, 6 mg for the fossil feathers, and 16 mg for the sediment. Curie point pyrolysis was carried out with a Pilodist Curie flash pyrolyser. Samples were heated at their Curie temperature for 10 s under a He flow of 1 ml/min. The instrument was coupled directly to a GC-MS system. The pyrolysis products were separated using a Trace Thermo gas chromatograph equipped with a Rxi5-SilMS column (30 m × 0.25 mm i.d., 0.5 μm film thickness). He was used as carrier gas at constant pressure of 15 psi. The injector temperature was 280°C in splitless mode. The oven temperature was maintained at 50°C for 10 min and was progressively increased to 310°C at 2°C/min. Coupled to the gas chromatograph was a DSQ Thermo mass spectrometer with a heated interface (310°C), electron energy of 70 eV and ion source at 220°C, scanning from *m/z* 35 to 800 at 2 scans/s. Compounds were assigned on the basis of their mass spectra, comparison with the NIST library mass spectra, published mass spectra (Gallois *et al.* 2007; Templier *et al.* 2013) and GC retention times. The molecular structure of all compounds present in substantial amount was investigated without any ion selection that could have biased interpretations.

Institutional abbreviations. NIST, National Institute of Standards & Technology, US Department of Commerce; RBINS, Royal Belgian Institute of Natural Sciences, Brussels, Belgium; YFGP, Yizhou Fossil & Geology Park, China.

RESULTS

SEM/EDS and XRD

SEM of the fossil feathers revealed that they are embedded in a sedimentary matrix containing mainly quartz, carbonates, and phyllosilicates. The latter are organized in thin platelets oriented parallel to each other (Fig. 2A, B). A feather sample from the right wing of *Anchiornis* (sample 1 on Fig. 1) showed abundant rounded crystals that are present only beneath the surface. They occur mainly as framboids (Fig. 2C), but also as individual microcrystallites (Fig. 2D) and, in some cases, are associated with voids. Framboids are spheroidal or ovoid, 6–9 μm in diameter and contain dozens of euhedral crystals, 750 nm in diameter. In contrast, individual cubic crystals are much smaller

(about 500 nm³) and contain micro-crystallites (Fig. 2D). EDS analyses indicate that the sediment is composed of Fe, Si, O, Al, C, Ca (and Mn, K, Mg), probably indicating the presence of quartz, calcite, and various phyllosilicates. XRD analyses confirmed the presence of these minerals in the sediment (Fig. 3A). In addition, the XRD spectrum of the <2 µm phase shows that expansive material, such as inter-stratified illite/smectite, is present in the sediment (Fig. 3B). Due to their characteristic framboidal shape and elemental composition, the crystal clusters observed beneath the fossil feather surface are attributed to diagenetic iron oxides or hydroxides. Indeed, although the framboidal habit is common for iron sulphides, the lack of S here shows they are rather iron oxide pseudomorphs probably resulting from the *in situ* weathering of pyrite framboids (Nordstrom 1982; Kaye *et al.* 2008; Wang *et al.* 2012; Blanco *et al.* 2013). These structures are associated with thin clay overgrowths (arrow in Fig. 2C, E), indicating that the iron oxides (or the preceding pyrites) precipitated first. Tiny stellate minerals were also observed and identified as probable iron oxides by x-ray spectroscopy (Fig. 2F). The presence of calcium carbonates, feldspars (Fig. 2G) and quartz (Fig. 2H) in the sedimentary matrix was confirmed by x-ray spectroscopy.

Elongate microbodies, 650–950 µm, and their associated imprints were observed in three samples (6, 9 and 12 on Fig. 1) collected from the anterior and posterior parts of the dinosaur tail (Fig. 4). Microbody imprints are abundant, tightly packed together and randomly oriented (Fig. 4A, B). They probably represent traces of melanosomes. Similar microbodies interpreted as melanosomes have previously been observed in feathers from the crest of this specimen (YFGP-T5199; Lindgren *et al.* 2015). Here, isolated elongate structures were observed (Fig. 4C). These fossil organelles are preserved within the thin clay-rich sediment.

Ion beam analysis: EBS and PIXE

The great virtue of EBS is to be capable of yielding the elemental depth profiles non-destructively from the outermost microns of the sample with good sensitivity and depth resolution (Jeynes & Colaugh 2016). A typical EBS spectrum obtained from the fossil feathers is shown in Cincotta *et al.* (2020, fig. S3) together with its best fit. The experimental spectrum was inverted to recover the elemental depth profiles (examples are shown for carbon in Cincotta *et al.* 2020, fig. S4). Integration of these elemental depth profiles allows derivation of the concentration of each element at a given depth. Figure 5A clearly shows that the C enrichment in the near surface region (*c.* 60%) decreases at increasing distance from the fossil feathers, reaching a minimum in the ‘remote’ sediment

(*c.* 14%). Sample concentrations of O and Si (although less obvious) follow an opposite trend. The N content in the modern buzzard feathers is *c.* 20–26%. The very low content of N in the fossil (*c.* 5%) and even less (under the limit of detection) in the remote sediment (Cincotta *et al.* 2020, fig. S3) precluded its depth profiling.

In contrast, EBS analysis of modern buzzard feathers shows homogeneous concentrations with depth (Cincotta *et al.* 2020, fig. S5). In the buzzard feathers, C content is about 60 at.%, while N and O are both around 20 at.% for the rachis and around 25 and 15 at.% respectively for the barbs. Typical PIXE spectra acquired from the fossil feathers, ‘host’ sediment and ‘remote’ sediment are shown in Figure 5B. The samples differ in the amounts of several elements present (Cincotta *et al.* 2020, tables S1, S2). Of particular interest is the S content: there are elevated concentrations of S in the fossil feathers (average 1842 ± 208.5 ppm), less in the ‘host’ sediment (1162 ± 143 ppm), and much lower concentrations in the ‘remote’ sediment (98 ± 35 ppm). The concentration of S in the fossil feathers is roughly 20 times lower (*c.* 0.2 wt.%) than in the modern bird feathers (*c.* 3.7–4.3 wt.%). The co-occurrence of S and C is also highlighted (Table 1). Both concentrations decrease with depth within the fossil feathers whereas the reverse situation is observed for Si and O.

¹³C NMR

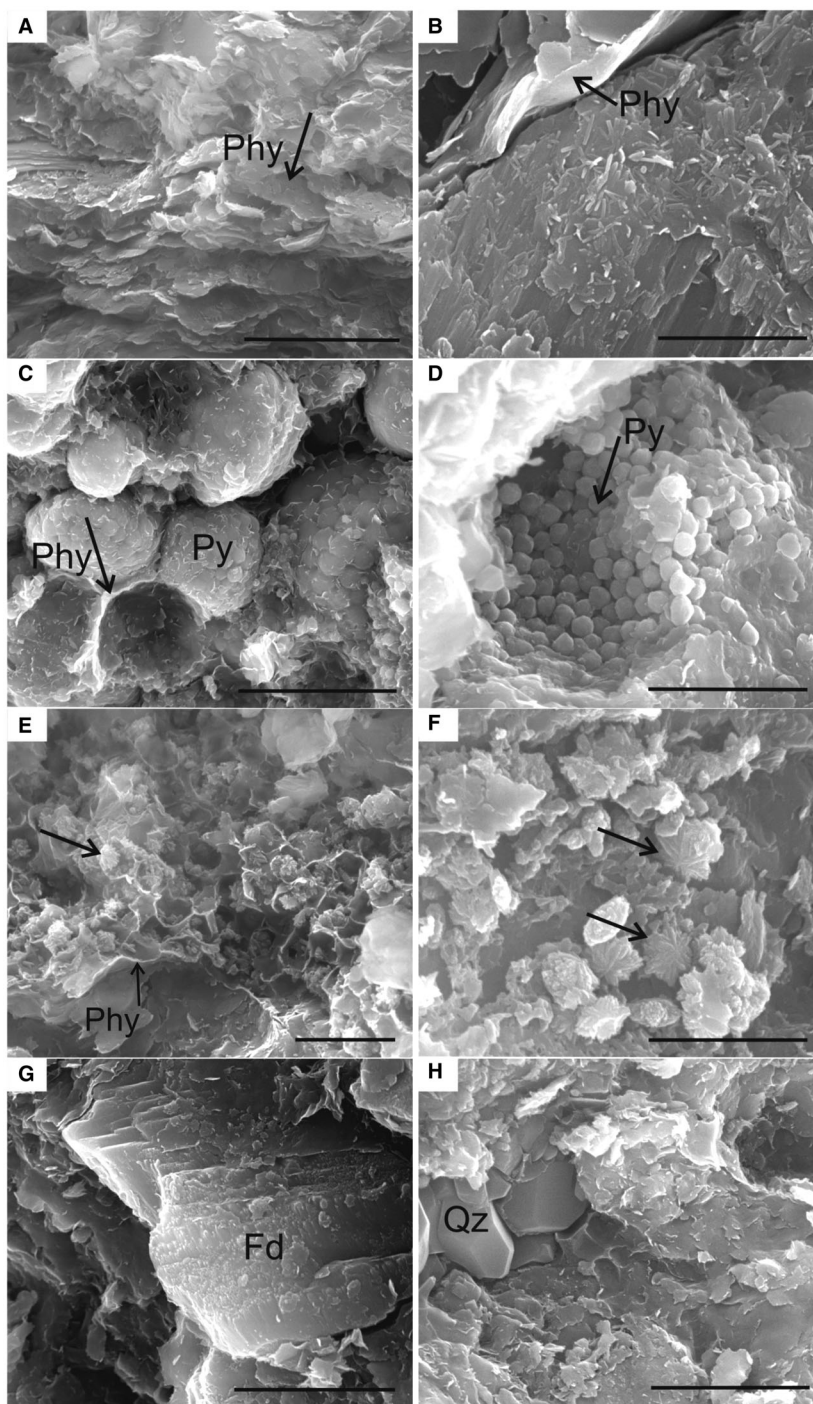
The ¹³C NMR spectrum of buzzard feathers (Fig. 6A) shows a complex signal in the aliphatic region, with well-resolved peaks between 10 and 65 ppm and a narrow peak at 173 ppm, due to carboxyl carbons, that is carboxylic groups and esters, and amides. Two additional, less intense, signals can be seen at 129 and 158 ppm in the unsaturated/aromatic carbon region. In comparison to the spectrum of modern feathers, the ¹³C NMR spectra of the fossil feathers and their surrounding sediment show much simpler patterns (Fig. 6B, C). The spectra are similar to each other and both are dominated by a broad peak in the aliphatic region, maximizing at 30 ppm and thus indicative of long alkyl chains. Two additional broad signals contribute to the spectra. The first one occurs as a broad shoulder between 68 and 80 ppm, in the O-alkyl C and N-alkyl C range, and the second one is a broad peak at 129 ppm, attributed to aromatic carbons.

Micro-ATR FTIR spectroscopy

The micro-ATR FTIR spectra of the theropod feathers, the embedding sediment and the modern buzzard feather (dark regions) are shown in Figure 7.

FIG. 2. Scanning electron microscopy (SEM) images of minerals observed in the plumage of *Anchiorhis huxleyi*. A–B, thin platelets of phyllosilicates observed in sample 7 (see Fig. 1 for location). C, pyrite framboids (sample 1). D, pyrite crystallites (sample 1). E, clayed pores containing small star-shaped iron-oxide crystals (sample 8). F, star-shaped iron oxides (sample 1). G, feldspar crystal surrounded by clay sheets (sample 5). H, quartz crystals embedded in a clayed matrix (sample 9). Arrowheads indicate the aforementioned minerals.

Abbreviations: Fd, feldspar; Phy, phyllosilicate; Py, pyrite; Qz, quartz. Scale bars represent: 5 μm (A, D, G, H); 3 μm (B); 10 μm (C); 2 μm (E, F).



The spectrum of the dark region of a modern buzzard feather shows characteristic bands of secondary amides (as in proteins and polypeptides) at 1628 cm^{-1} (C=O stretch of Amide I), 1531 cm^{-1} (C–N stretch, Amide II) and 1239 cm^{-1} (N–H in plane bending coupled with C–N stretch, Amide III). Broad bands around 3274 and 3125 cm^{-1} can be attributed to the N–H stretching of secondary amides. The bands at 2961 , 2922 and 2852 cm^{-1}

are assigned to the C–H stretching of methylene and methyl groups. These two spectra are very similar and no significant differences could be found between IR response of the dark and white regions of the same feather.

The spectrum of the fossil feathers has a different pattern but some similarities with the modern buzzard feather appear. The distinct bands at 2920 and 2851 cm^{-1} can also be attributed to C–H stretching of methylene

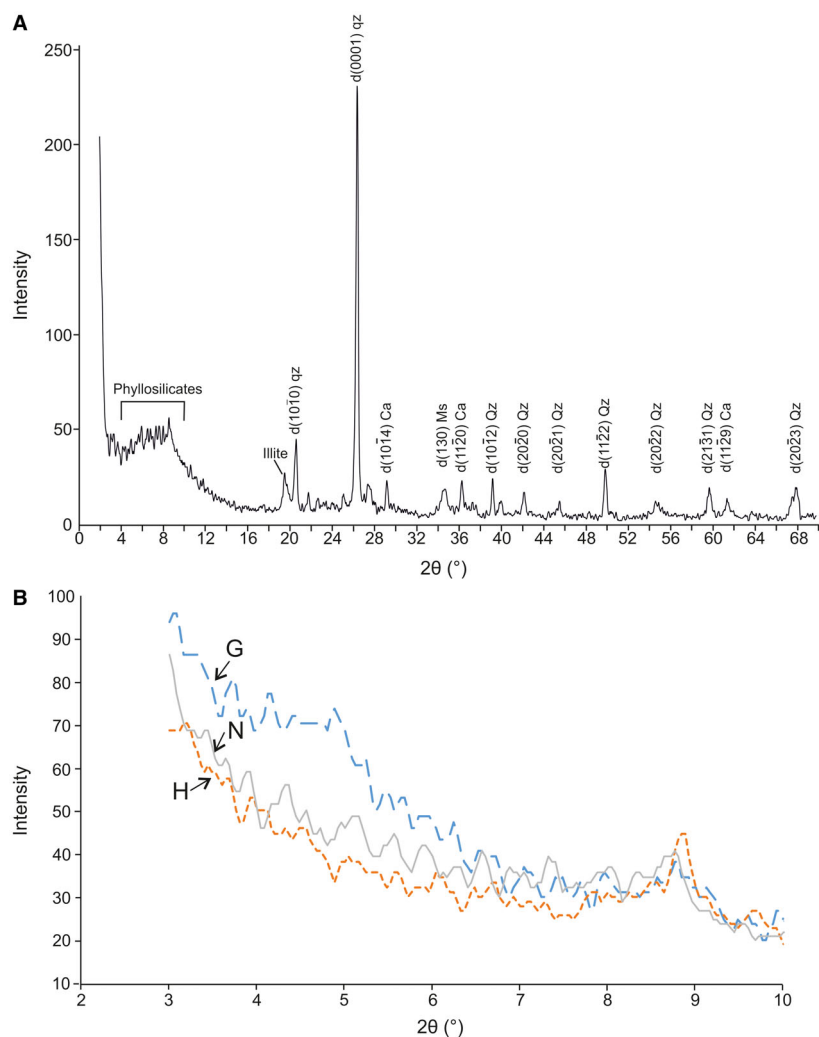


FIG. 3. X-ray powder diffraction patterns of the ‘host’ sediment. A, spectrum of the bulk rock; ca, calcite; qz, quartz. B, the fraction $<2\ \mu\text{m}$, with spectra of natural (N), glycolated (G), and heated (H) sample; the expansive illite/smectite interstratifications can be observed in the spectrum of the glycolated (G) material through shifts in the position of the peaks. Colour online.

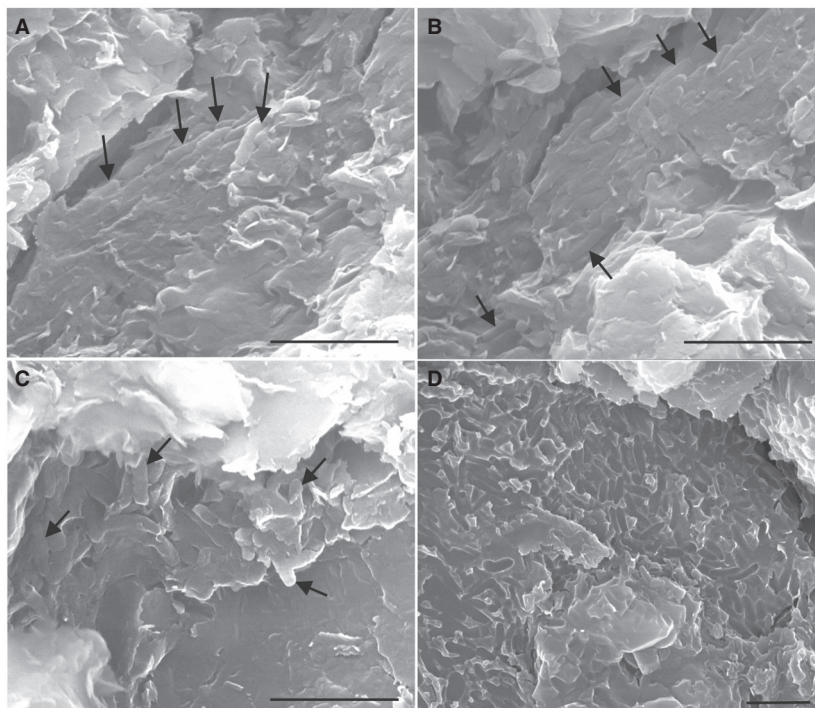
and methyl groups. These associated bands are also present in the IR spectrum of the surrounding matrix but with different relative intensities. A broad region around $3300\ \text{cm}^{-1}$ is present, although much less marked, and is indicative for O–H stretching as found in carboxylic groups and alcohols. In the spectra of the fossil feathers, a broad band at about $1560\ \text{cm}^{-1}$ can be attributed to carboxylate. This band is not present in the IR spectrum of the sediment. Another broad band around $1412\ \text{cm}^{-1}$ is found in the spectrum of the fossil feathers and might be related to the presence of CaCO_3 overlapping with C–H bending vibrations at 1460 and $1380\ \text{cm}^{-1}$ (Andersen & Brečević 1991; Kröner *et al.* 2010; Kiros *et al.* 2013). This is also confirmed by the presence of weak bands at 873 and $718\ \text{cm}^{-1}$. The IR spectrum of the sediment shows a similar, but less defined, absorption band between 1415 and $1463\ \text{cm}^{-1}$. The IR spectrum of the

fossil feathers and its surrounding matrix both show a narrow band at $1260\ \text{cm}^{-1}$ that could be attributed to the Si–CH₃ vibrations. Both spectra show an intense broad band at $1013\ \text{cm}^{-1}$ together with the weaker bands at 873 and $797\ \text{cm}^{-1}$ related to the sedimentary matrix (clay minerals, quartz, silicates, Si–O stretching). The IR spectrum of the sedimentary matrix shows an additional band at $720\ \text{cm}^{-1}$ that is also present, although very weak, in the fossil, indicating long-chain alkyl groups (CH₂ rocking vibrations). All the peaks mentioned above are absent in the IR spectra of the modern feather.

TMAH Py-GC-MS

Pyrochromatograms were obtained for the three following samples: the modern and fossil feathers, and the ‘host’

FIG. 4. SEM images of the ultra-structure of *Anchiornis* plumage. A–B, elongated microbodies (arrows) observed in sample 6 (see Fig. 1 for location). C, elongated microbodies (arrows) observed in sample 9. D, imprints observed in samples 6. All scale bars represent 2 μm .



sediment. In agreement with previous studies on bird feathers (Brebu & Spiridon 2011; Saitta *et al.* 2017), the pyrochromatogram of the modern feathers is dominated by cyclic molecules containing N, along with methylbenzene **1**, methylbutane nitriles **2**, **3** and cyclohexanedione **11** derivatives (Fig. 8A). Detailed interpretation of mass spectral fragmentation patterns allowed identification of the major pyrolysis products (Table 2) and further assignment to possible source. Molecular structures are given in Appendix 1, with methyl groups added by TMAH indicated in bold. Products **6**, **8**, **10** result from direct methylation of alanine, valine and proline, thus pointing to a proteinaceous origin for the feathers. This is further supported by the occurrence in substantial amounts of alkyl nitriles **2**, **3** resulting from dehydration of amides involving isoleucine and leucine, respectively, and of methoxybenzenes **7**, **9** released through homolysis of the side chain of tyrosine (Ratcliff *et al.* 1974). Methylbenzene **1**, pyrrole **4** and ethylbenzene **5** are rather ubiquitous pyrolysis products in sedimentary organic matter. However, they can also be released upon pyrolysis of phenylalanine and serine (Gallois *et al.* 2007). Mass spectral fragmentation pattern (base peak at m/z 82) suggests an origin from the side chain of histidine for compound **16**. Similarly, compound **17** probably corresponds to a valine derivative as its mass spectrum is characterized by the loss of 42 amu (i.e. valine side chain). Dimethylcyclohexanedione **11** was reported as pyrolysis product of glycine (Moldoveanu 2009). Glycine is also present as its diketopiperazine **15** resulting from combined dehydration and cyclization (Simmonds *et al.* 1972).

The same mechanism involving two different amino acids (isoleucine–glycine) leads to another diketopiperazine **18** (Hendrick & Voorhees 1996). The formation of more complex diketopiperazines was proposed by Templier *et al.* (2013) from tripeptide units. A similar mechanism can be invoked for the formation of compound **19** from valine, as well as compounds **20** and **21** from serine and leucine (Table 2; Cincotta *et al.* 2020, fig. S6). Imidazolidinedione **12** probably results from the internal cyclization of tripeptide comprising an alanine unit as reported by Templier *et al.* (2013; Cincotta *et al.* 2020, fig. S6). The formation of imidazolidinone **13** can be related to the decomposition of bicyclic amidine derived from valine as suggested by Basiuk & Navarro-González (1997; Cincotta *et al.* 2020, fig. S6). Another decomposition pathway of bicyclic amidine is probably responsible for the formation of imidazolidinone **14** from valine and possibly glycine (Templier *et al.* 2013). As far as we know, this is the first identification of such complex molecules (diketopiperazines from tripeptide and imidazolidinone from bicyclic amidine) in the pyrolysate of a natural sample.

By comparison, pyrochromatograms of the fossil feathers and their ‘host’ sediment are simpler. They are dominated by *n*-alkane/*n*-alkene doublets (Fig. 8B, C), resulting from the homolytic cleavage of long alkyl chains. In the fossil feathers, these doublets comprise from 8 to 30 carbon atoms, and exhibit a smooth distribution except for an intense C_{18} doublet. An additional series of fatty acid methyl esters with alkyl chain ranging from C_8 to C_{30} and maximizing at C_{16} is also identified (Table 2). It results

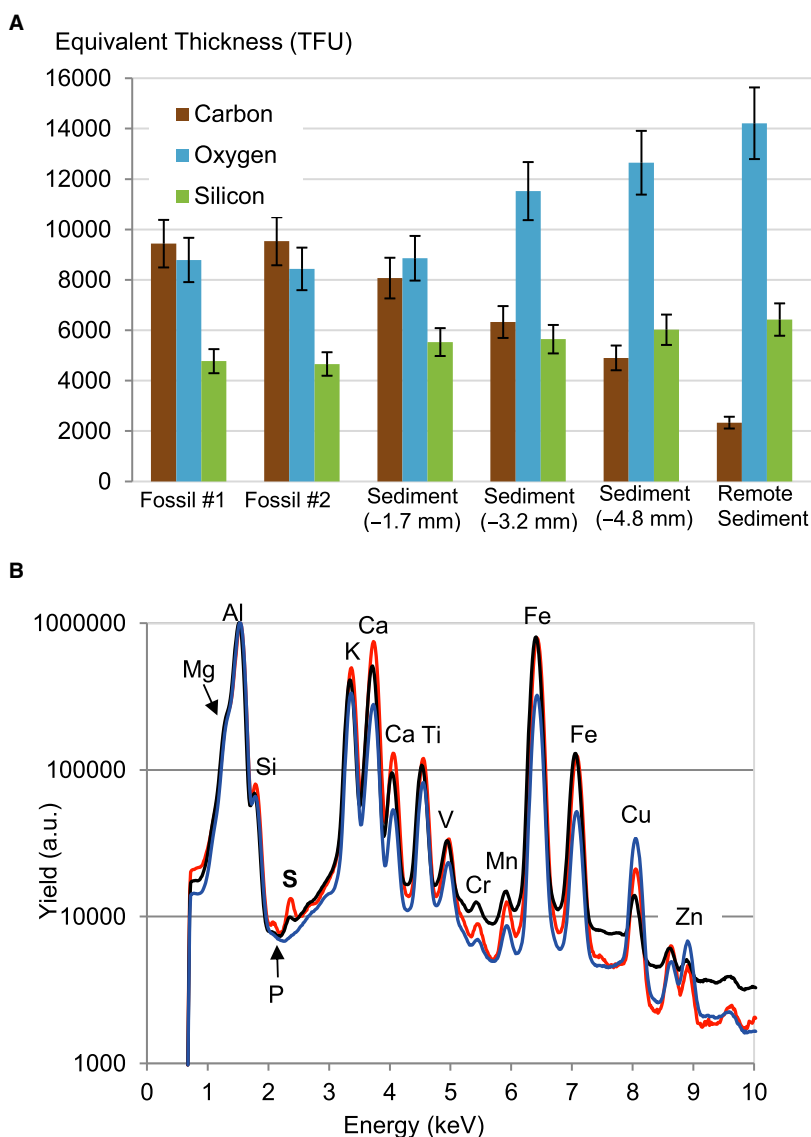


FIG. 5. Results of elastic backscattering spectrometry (EBS) and particle-induced x-ray emission (PIXE) analyses on the fossil feathers, the 'host' sediment and the 'remote' sediment. A, global content of C, O and Si obtained by EBS, in integrating the C, O and Si depth profiles over the 0–25 000 TFU interval; error bars give an estimate of the uncertainties considering the counting statistics as well as the cross-section and stopping power uncertainties; analysis was performed in duplicate on the same area of the fossil feather (Fossil #1, Fossil #2), three points of analysis were taken at three different locations in the 'host' sediment (at 1.7, 3.2 and 4.8 mm from the fossil), and one in the remote sediment. B, PIXE spectra obtained for one point of analysis in the fossil feather (red), the 'host' sediment (black), and the remote sediment (blue); the spectra are normalized to the Al signal (which comes mainly from the selective filter) to allow for a direct comparison.

from the release on pyrolysis of a series of fatty acids that are methylated thanks to TMAH. In addition to these series, a methoxybenzene substituted by two methyl groups or an ethyl group **22** is detected in minor amounts, at the beginning of the pyrochromatogram. A trimethylbenzene and a methylated derivative of methoxyaniline **23** also contribute to this part of the pyrochromatogram. However, the most prominent pyrolysis product **24** corresponds to the C₁₈ alcohol methylated through TMAH pyrolysis.

The pyrochromatogram of the 'host' sediment shares several similarities with that of the fossil feathers. Indeed, it is dominated by series of alkane/alkene doublets and fatty acid methyl esters. Although the distribution of the fatty acid methyl esters is similar in both samples, that of the doublets differs. Indeed, whereas their range (C₈–C₃₀) is similar, the maximum of the series appears at C₁₅ in

the sediment, instead of a marked predominance of the C₁₈ in the fossil (Table 2). Moreover, when comparing the minor compounds eluting at the beginning of the pyrochromatogram, compounds **22** and **23** are common in both samples, whereas a higher number of alkylbenzene homologues occurs in the sediment. Finally, the contribution of octadecanol **24** is much lower in the sediment pyrolysate.

DISCUSSION

Ultrastructure

Microbodies and elongate moulds are observed in feather samples collected at three different locations on the

TABLE 1. PIXE derived concentration data for S and C in the fossil and modern feathers, and 'host' sediment.

	[S] (ppm)	[C] (ppm)
Fossil Feather #1	1739	80 385
Fossil Feather #2	1946	82 171
+1.7 mm*	1162	72 012
+3.2 mm*	801	49 213
+4.8 mm*	893	41 835
Remote sediment	98	20 331
Rachis	37 142	547 174
Barbs	43 070	314 962

*distance of the analysed spot from the feather/sediment boundary.

See Cincotta *et al.* (2020, table 1) for details on the global uncertainty calculations, Fig. 1 and Cincotta *et al.* (2020, fig. S2) for the location of the analyses.

Anchiornis tail. The elongate shape, parallel orientation and location of the microbodies within the feathers strongly suggest that they correspond to eumelanosomes. These pigment organelles are associated to brown, grey and black hues in modern bird feathers. The preservation of melanosomes, and especially eumelanosomes, in dinosaur feathers is not uncommon. Such microscopic melanin-bearing structures have been described in other theropod dinosaurs, basal birds and isolated feathers (Li *et al.* 2010, 2012; Zhang *et al.* 2010; Carney *et al.* 2012; Colleary *et al.* 2015; Pan *et al.* 2016; Hu *et al.* 2018). The chemical composition of these microbodies has been assessed in a previous study, confirming a melanosome origin (Lindgren *et al.* 2015).

Recent taphonomic experiments in abiotic conditions suggest that the preservation of mouldic melanosomes requires interaction with an oxidant prior to maturation, and that the preservation of melanosomes is probably less frequent than the preservation of keratinous structures in fossil feathers (Slater *et al.* 2020). Interestingly, *Anchiornis* feathers contain both melanosomes and moulds. The nature of the former experiments does however not reflect the depositional and fossilization conditions of *Anchiornis*.

Depth profiling, light and heavy element composition

The C and N concentrations determined by EBS led to N/C ratios of 0.33–0.42 in modern buzzard feathers, and of 0.08 for the fossil, suggesting a marked relative decrease in N. The C concentration gradient observed by EBS in the fossil feathers of *A. huxleyi* strongly suggests that they are preserved as carbonaceous layers located in the uppermost part of the sample (i.e. 0–3 μm depth, given a rock density of 2.65 g/cm³) and suggests that

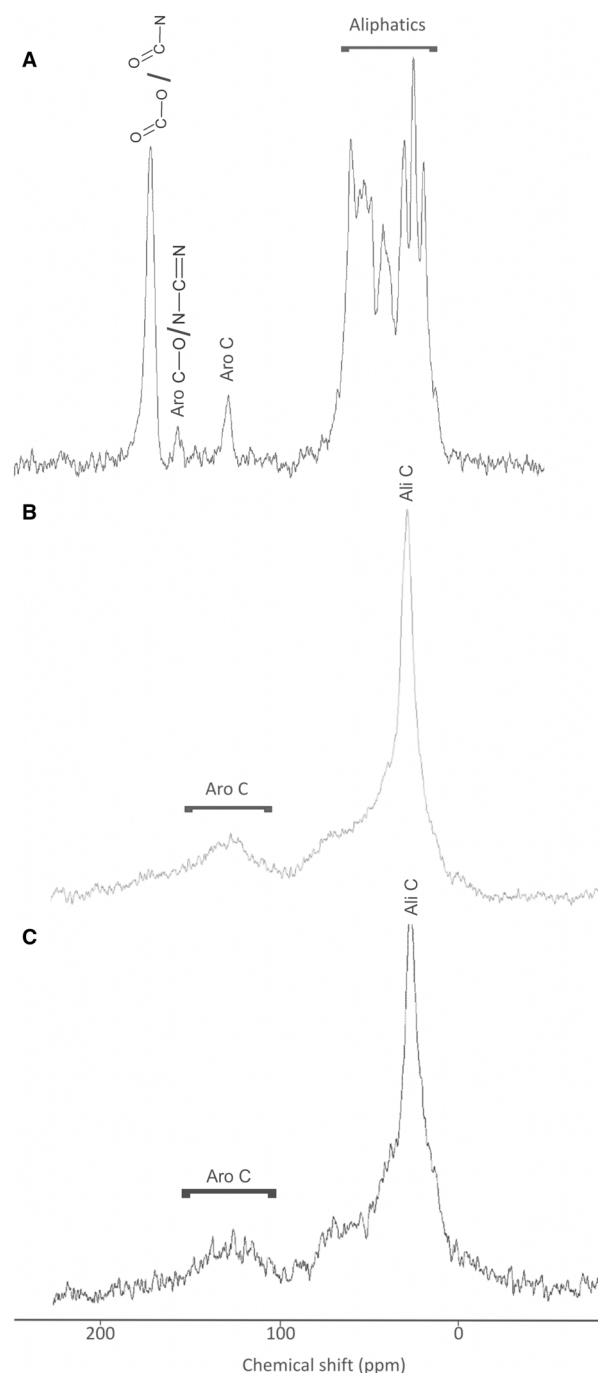


FIG. 6. Cross polarization/magic angle spinning ¹³C nuclear magnetic resonance (CP-MAS ¹³C NMR) spectra of: A, the modern bird feather; B, the fossil feathers; C, the 'host' sediment. Major chemical functions are indicated on each peak.

fossil organic matter could have impregnated the sediment only in a nearby area.

The PIXE spectra show elevated concentrations of S in the fossil feathers and, to a lesser extent, in the 'host' sediment, together with very low concentrations in the

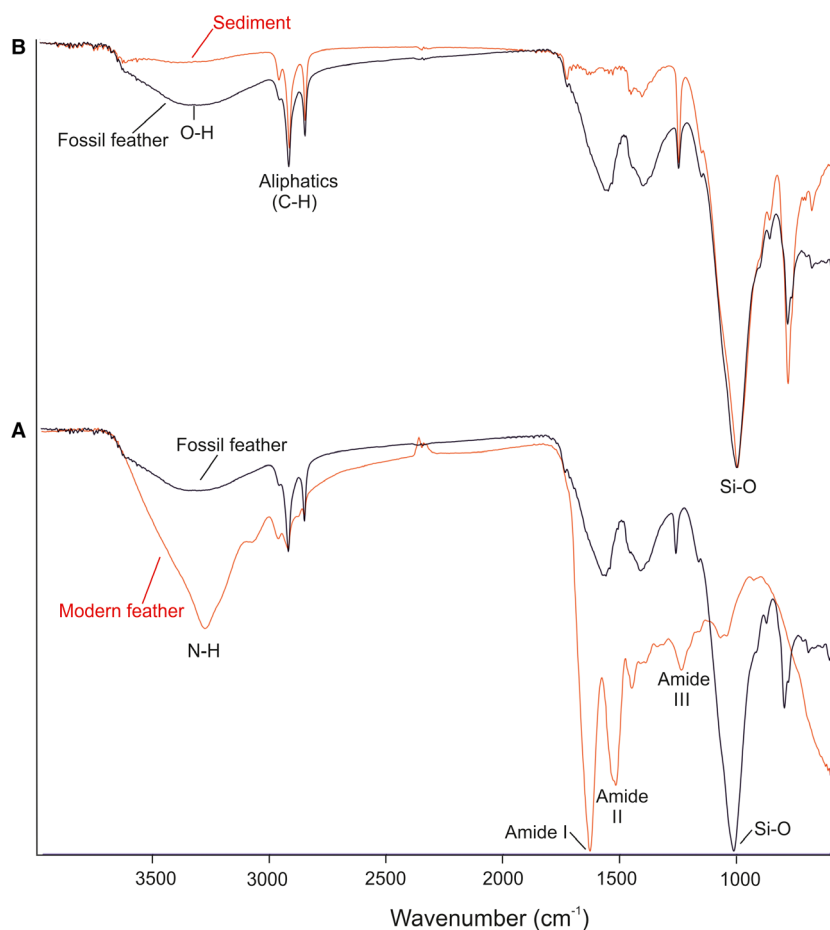


FIG. 7. IR spectra showing the comparison of: A, a modern buzzard feather with *Anchiornis* feathers; B, *Anchiornis* feathers with the sedimentary matrix ('remote' sediment). See the text for peak assignment. The spectra are normalized to 100% transmittance. Colour online.

'remote' sediment. This suggests that S is associated with the soft tissues. The fossil feathers are therefore preserved as a S-rich carbonaceous film. Substantial quantities of S are present in the modern buzzard feathers ($43\,070 \pm 4236$ ppm in the brown barbs and $37\,142 \pm 3652$ ppm in the rachis, Table 1). This is not surprising due to the presence of S-containing biomacromolecules, such as the pigment phaeomelanin and proteins containing cysteine or methionine (i.e. keratins) in bird feathers (Harrap & Woods 1964; Murphy *et al.* 1990; Cesarini 1996; Riley 1997; Bortolotti 2010; Saravanan & Dhurai 2012). Important studies on the chemical composition of feathers have shown that S is a major element of bird feathers (Harrap & Woods 1964, 1967; King & Murphy 1987; Murphy *et al.* 1990; Edwards *et al.* 2016). Some authors could even discriminate between organic S originating from keratin and phaeomelanin based on its speciation (Edwards *et al.* 2016). Previous *in situ* chemical analysis (time-of-flight secondary ion mass spectrometry; TOF-SIMS) of the melanosomes from the present fossil revealed their enrichment in S with respect to the surrounding sediment, but it could not determine whether it reflects the occurrence of phaeomelanin or diagenetic incorporation of S in eumelanin (Lindgren *et al.* 2015). It

has been suggested that divalent elements (Cu, Ca, Zn) formed chelates with melanin in a Cretaceous early bird (Wogelius *et al.* 2011). Such a complexation may have played a role in S-preservation in fossil soft tissues. Alternatively, the presence of S in the fossil feathers can be attributed to natural sulphurization of the organic matter, that is the abiogenic intra-molecular incorporation of S from the depositional environment during early diagenesis. The incorporation of S into organic matter was interpreted as a way to enhance the preservation potential of certain labile substances through cross-linking (Sinninghe-Damsté *et al.* 1988, 1989; Sinninghe-Damsté & De Leeuw 1990; McNamara *et al.* 2016). Indeed, organic matter has the ability to form complexes with inorganic elements, including S, which was traced in fossil soft tissues (Wogelius *et al.* 2011).

Functional groups in the organic matter

On the whole, the ^{13}C NMR and IR spectra of buzzard feathers (Figs 6A, 7A) are comparable to that of several keratinous materials, such as feather keratin (Kricheldorf & Müller 1984; Barone *et al.* 2005; Wang & Cao 2012,

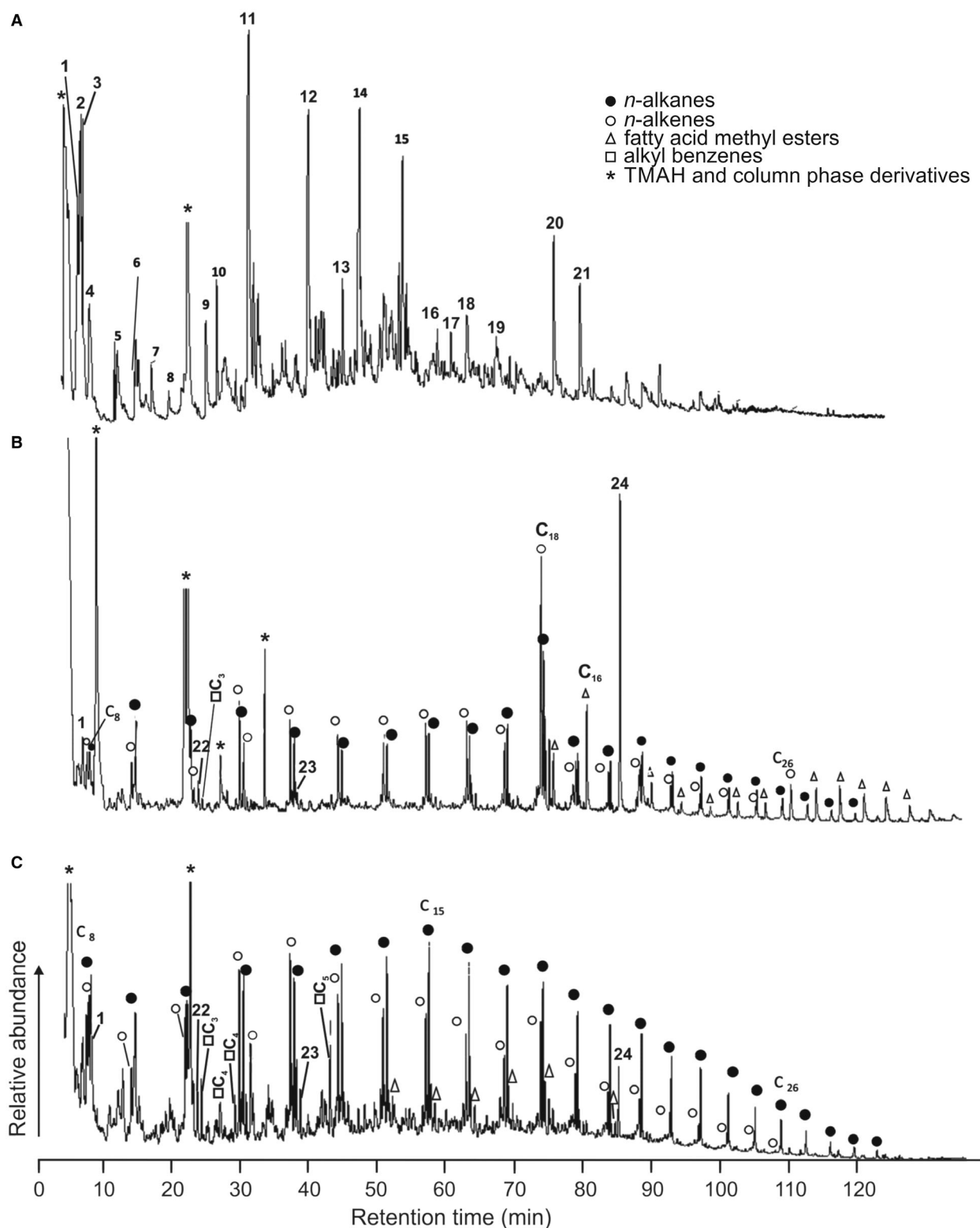


FIG. 8. Chromatograms of the products formed during the pyrolysis of: A, modern buzzard feathers; B, fossil feathers; C, remote sediment. Peak identifications are given in Table 2. C_n , carbon chain, with n indicating the length of the chain.

TABLE 2. Main products released from pyrolysis of modern feathers, fossil feathers and embedding sediment in the presence of TMAH.

Peak	Retention time (min)	Major characteristic ions ^a (m/z)	Molecular ion	Compound	Possible origin ^b	Modern feather	Fossil feather ^c	Embedding sediment ^c
1	6.7	<u>91</u> ; 92; 39; 65	92	Methylbenzene	(Phe)	X	X	X
2	6.9	<u>55</u> , 54, 42	83	2-methylbutanenitrile	Ileu	X		
3	7.1	<u>43</u> , 41, 39, 68	83	3-methylbutanenitrile	Leu	X		
4	8.0	<u>67</u> ; 41; 39; 40	67	1 <i>H</i> -Pyrrole	(Ser)	X		
5	12.1	<u>91</u> ; 55; 106; 65	106	Ethylbenzene	(Phe)	X		
6	14.8	<u>72</u> ; 42; 56; 131	131	N,N- Dimethylalanine methylester	Ala	X		
7	17.0	<u>108</u> ; 78; 65; 39	108	Methoxybenzene	Tyr	X		
8	19.5	<u>86</u> ; 102; 42; 55	145	N-Methyl-valine methyl ester	Val	X		
9	25.0	<u>122</u> ; 77; 107; 91	122	1-Methoxy-4-methylbenzene	Tyr	X		
10	26.5	<u>84</u> ; 42; 100; 58	143	N-Methyl-proline methyl ester	Pro	X		
11	31.2	<u>56</u> ; 140; 42; 112; 83	140	2,5-Dimethylcyclohexane-1,4-Dione	Gly	X		
12	39.7	<u>42</u> ; 127; 142; 56	142	1,3,5-Trimethylimidazolidine-2,4-Dione	Ala?	X		
13	44.8	<u>56</u> ; 126; 139; 41	182	1-Isobutyl-4-isopropylimidazolinone	Val	X		
14	47.2	<u>128</u> ; 42; 71; 113	170	5-Isopropyl-1,2,3-trimethylimidazolidinone	Val-(Gly)	X		
15	53.6	<u>128</u> ; 42; 57; 71	128	1-Methylpiperazine-2,5-dione	Gly	X		
16	58.6	<u>82</u> ; 167; 182; 110	182	?	His?	X		
17	60.5	<u>152</u> ; 41; 55; 137; 179	194	?	Val?	X		
18	62.9	<u>142</u> ; 113; 42; 71	198	1-Methyl-3-(1-methylpropyl)piperazine-2,5-dione	Ileu-Gly	X		
19	67.1	<u>142</u> ; 113; 42; 98; 212	?	N-(1-oxo-2-amino-3-methylbutyl)piperazine-2,5-dione derivative	Val	X		
20	75.5	<u>139</u> ; 70; 42; 168	210	N-Methyl-3-methylidene-6-(3-methylbutyl)piperazine-2,5-dione	Ser-Leu	X		
21	79.2	<u>168</u> ; 139; 70; 42	210	Isomer of compound 20	Ser-Leu	X		
22	23.7	<u>136</u> , 121, 122, 91	136	1-Methoxy-2,3-dimethylbenzene or 1-Ethyl-2-methoxybenzene	Lignin or cellulose		X	X
23	38.1	<u>136</u> , 122, 137	137	Methoxy-methylaniline	?		X	X
24	86.3	<u>45</u> ; 57; 97; 224; 252	284	1-Methoxyoctadecane	?		X	X
●		<u>43</u> ; 57; 71; 85		<i>n</i> -alkanes	Aliphatic chains		C ₈ -C ₃₀ (C ₁₈ , C ₁₁)	C ₈ -C ₂₉ (C ₁₅)
○		<u>55</u> ; 43; 69; 83, 97		<i>n</i> -alk-1-enes	Aliphatic chains		C ₈ -C ₂₆ (C ₁₁ , C ₁₈)	C ₈ -C ₂₉ (C ₁₁ , C ₁₈)
Δ		<u>87</u> ; 74; 43; 55		Fatty acid methyl esters	Aliphatic chains		C ₈ -C ₃₀ (C ₁₆)	C ₈ -C ₃₀ (C ₁₆)
□		91, 105		Alkyl benzenes	?		C ₃	C ₃ -C ₅ (C ₅)

^aMS fragments are in order of decreasing abundance, with base peak underlined.^bCompounds in brackets indicate possible origin that is not univocal; Ala, alanine; Gly, glycine; His, histidine; Ileu, isoleucine; Leu, leucine; Phe, phenylalanine; Pro, proline; Ser, serine; Tyr, tyrosine; Val, valine; ? tentative origin.^cC_{range} (C_{max}, C_{submax}).

Sharma *et al.* 2018), wool keratin (Yoshimizu & Ando 1990; Wojciechowska *et al.* 2004) or gecko setae keratin (Jain *et al.* 2015). Indeed, the peak at 173 ppm should mainly correspond to the signal of secondary amide (O=C–NH) groups involved in the peptidic bonds. This is confirmed by the presence of characteristic bands of secondary amides in the IR spectrum of the brown feathers (Fig. 7A). This includes a broad band around 3277 cm^{-1} attributed to the N–H stretching band of amides, a narrow band at 1628 cm^{-1} related to the C=O stretch of Amide I, a band at 1518 cm^{-1} attributed to Amide II and a band at 1237 cm^{-1} related to Amide III (Bendit 1966; Yu *et al.* 2004; Wang & Cao 2012; Giraldo & Moreno-Piraján 2013; Tesfaye *et al.* 2017).

Carbon atoms bearing both COOH and NH₂ groups (termed C_α) in the amino acids (except glycine) resonate between 50 and 60 ppm in ¹³C NMR. They account for the peaks at 52.9 and 60.2 ppm in the broad aliphatic signal, whereas the signal at 42.6 ppm is assigned to the C_α of glycine. The other peaks are mainly associated with the amino acid side chains, that at 30.8 ppm being assigned to C_β along with C in long alkyl chains, and those at 19.8 and 25.7 ppm to C_γ and C_δ. The three bands located in the 2961–2850 cm^{-1} range in the IR spectrum confirms the presence of aliphatic moieties in the modern feathers, although their precise assignment to dedicated compounds is uncertain. In the ¹³C NMR spectrum, the 129 ppm peak is typical for aromatic carbons, including those from phenylalanine and tyrosine (Yoshimizu & Ando 1990; Jain *et al.* 2015). Finally, the peak at 158 ppm can be ascribed to the O-alkyl C of tyrosine and/or the C of the guanidino group (N–C=N) of arginine (Yoshimizu & Ando 1990; Jain *et al.* 2015). This spectrum is in agreement with previous reports indicating that keratin is a major constituent of feathers (Lucas & Stettenheim 1972). The ¹³C NMR and IR spectra of the modern feathers also shares some similarities with various types of melanins (Ito & Nicol 1974; Duff *et al.* 1988; Adhyaru *et al.* 2003; Centeno & Shamir 2008).

The much simpler ¹³C NMR spectra of the fossil feathers and their surrounding sediment are dominated by long alkyl chains with a low contribution of aromatic carbons. This is also consistent with the IR spectra (Fig. 7B), mainly showing contributions of aliphatics and silicate and carbonate minerals. When compared to the ¹³C spectrum of the modern feathers, the aliphatic signal in the fossil is poorly resolved; the aromatic peak is broad and no resonance signal could be detected in the carboxylic region. These features suggest that the proteinaceous contribution identified in the buzzard feathers is no longer present in the fossil sample. The comparison between the FTIR spectrum of the modern feather and that of the fossil feathers (Fig. 7A) shows that the characteristic bands of amides are absent in the IR spectrum of the fossil

feathers. However, a more precise comparison can be achieved at the molecular level thanks to pyrolysis in the presence of TMAH coupled with GC-MS.

Molecular building blocks of organic matter

TMAH Py-GC-MS analysis of modern feathers thus highlights the presence of glycine, serine, leucine, alanine, valine and proline moieties in buzzard feather keratin, in agreement with previous studies on feather keratin (Fig. 8A; O'Donnell & Inglis 1974; Arai *et al.* 1983, 1986; Murphy *et al.* 1990; Staroń *et al.* 2011; Saravanan & Dhurai 2012). Additionally, pyrolysis products derived from isoleucine, phenylalanine and tyrosine occurred in substantial amounts although they are often considered as minor constituents of feather keratin. However, homolysis of the side chain of phenylalanine and tyrosine favours high yields in TMAH pyrolysis (Gallois *et al.* 2007). Despite its acknowledged high abundance in feather keratin, cysteine is absent in the pyrochromatogram of buzzard feathers, probably because it mainly releases H₂S on pyrolysis (Moldoveanu 2009), not detected in the presently used analytical conditions. Alternatively, some of the identified products (methylbenzene **1**, methyl, methoxybenzene **9**) as well as glycine derivatives may originate from melanin, although they are poorly diagnostic compounds (Stępień *et al.* 2009). However, the melanin signal was reported to be overwhelmed by protein-derived products upon pyrolysis of bulk feathers (Barden *et al.* 2011).

The pyrochromatograms of the fossil feathers and their 'host' sediment are comparable as they are both dominated by series of alkane/alkene doublets and fatty acid methyl esters as well as minor compounds eluting at the beginning of the pyrochromatogram. The latter include a methoxybenzene substituted by two methyl groups or an ethyl group **22** which originates from lignin or polysaccharides such as cellulose, depending on its substitution pattern (Seitz & Ram 2000; Choi *et al.* 2013). Despite these similarities, differences are observed, including the much weaker abundance of octadecanol **24** in the sediment pyrolysate. These differences clearly show that even though some imprint from the sediment may have contributed to the fossil feather pyrolysate, at least some features are typical for the fossil feathers. They notably include the C₁₈ doublet and octadecanol **24**. The predominance of the alkane/alkene doublets in the pyrolysate is in agreement with the strong aliphatic signal observed in NMR and FTIR (bands at 2690, 2920 and 2851 cm^{-1}) (Figs 6, 7). A similar highly aliphatic character has been reported in Eocene bird feathers (O'Reilly *et al.* 2017) but also in soft tissues from other fossil organisms, such as in cuticles from Carboniferous arthropods (Baas *et al.* 1995;

Stankiewicz *et al.* 1998), skin from a Cretaceous mummified hadrosaur (Manning *et al.* 2009) and Cretaceous fish scales (Gupta *et al.* 2008). C₁ to C₃ alkylbenzenes were also identified in pyrolysates of Oligocene weevil and tadpole, and associated matrix (Gupta *et al.* 2007; Barden *et al.* 2015).

The aliphatic series dominating the pyrolysate of the fossil feathers reflect either selective preservation of macromolecular aliphatic matter pre-existing in the extant organism (Tegelaar *et al.* 1989) or *in situ* polymerization of aliphatic lipids (Stankiewicz *et al.* 2000; Gupta *et al.* 2007). No such aliphatic series could be detected in the pyrolysate of modern feathers, probably precluding the first hypothesis. In contrast, several aliphatic series were identified in the lipid extract of the modern feathers (*n*-alkanes, *n*-acids, *n*-alcohols; data not shown). Indeed, modern bird feathers are coated by lipids as protection against adverse environmental factors. Such lipids, secreted by the uropygial gland, were shown to be preserved through geopolymerization in an Eocene bird (O'Reilly *et al.* 2017). A similar geopolymerization can be put forward to account for the occurrence of aliphatic moieties of the present fossil feathers. Endogenous lipids may be transformed into more stable geopolymers, composed of alkane/alkene doublets, and can therefore be 'preserved' and traced in vertebrate fossils (O'Reilly *et al.* 2017).

The absence of signals typical for proteinaceous material in the NMR and IR spectra and pyrochromatogram of the fossil feathers is noteworthy. It is further suggested by the weak N/C ratio in the fossil when compared with modern feathers. The lack of proteinaceous components consistent with keratin was previously suggested on the same fossil based on TOF-SIMS and IR analyses (Lindgren *et al.* 2015). In agreement with the commonly accepted lability of proteins, this feature suggests their extensive degradation in our specimen upon diagenesis. Recent taphonomy experiments on extant feathers demonstrated substantial degradation of keratin upon microbial and thermal decay (Saitta *et al.* 2017). Moreover, it must be noted that diagenetic degradation of proteinaceous moieties was previously put forward for Eocene birds (O'Reilly *et al.* 2017; Saitta *et al.* 2017) and Palaeozoic annelid fossils (Dutta *et al.* 2010). However, even if no proteinaceous compounds were detected in *Anchiornis* feathers, one cannot exclude the possibility of finding similar biomolecules preserved in other fossils in the future.

Although PIXE analyses showed that C and S are closely associated in the fossil feathers, no organosulphur compound could be detected in the pyrolysate. Altogether, the lack of organosulphur compounds (such as thiophenes) in the fossil feather pyrolysates and the lack of C=S/C-S species in their IR spectrum strongly suggest

a lack of organic-S species in this sample. In contrast, S incorporation was evidenced through FTIR and TMAH-Py-GC-MS in melanosomes of Miocene frogs, thus demonstrating involvement of natural sulphurization in the preservation of the fossil organic matter (McNamara *et al.* 2016). The lack of organosulphur compounds in *Anchiornis* pyrolysate should thus reflect diagenetic conditions that prevented such natural sulphurization of organic matter. In the sedimentary environment, the sulphurization of organic matter to form organosulphur compounds requires the presence of reactive organic matter and inorganic sulphides (i.e. anoxic conditions), with sufficient, but not excessive, reactive iron. If reactive iron exceeds a certain quantity, iron sulphides (pyrite) would precipitate instead (Canfield 1989; Werne *et al.* 2000). Here, our results suggest that the concentration of S and Fe in the environment was high enough to form iron sulphides (i.e. pyrite framboids and microcrystallites). The occurrence of iron oxides or hydroxides as framboid crystals (SEM and EDX characterization) suggests that S may have been preferentially used for the formation of iron sulphides (such as pyrite) during early diagenesis (Sinninghe-Damsté & De Leeuw 1990). During later diagenesis, pyrite framboids were probably weathered *in situ* into the iron oxides and hydroxides observed beneath the carbonaceous surface of feathers, thus releasing S that may have been further associated with organic compounds, for example through the formation of chelate with melanin (Wogelius *et al.* 2011). Such associations may have favoured/enhanced organic matter preservation and are consistent with the interrelation between S and C highlighted by PIXE analyses.

Recently, a mechanism of nitrogen preservation based on lipoxidation and glycoxidation of proteins was proposed in biomineralized tissues of diverse Mesozoic and Cenozoic vertebrates, fossilized in oxidative settings (Wiemann *et al.* 2018). Such a process, which can be catalysed by transition metal such as iron, may have led to the preservation of the small amount of nitrogen in YFGP-T5199. However, the present study deals with soft tissues and not biomineralized ones. Additionally, so far this preservation mechanism could only be evidenced in oxidizing environments (Wiemann *et al.* 2018). The occurrence of iron oxide framboids in the studied *Anchiornis* fossil probably resulting from pyrite weathering, rather attests for the reducing conditions of fossilization, thus making the involvement of this preservation pathway unlikely (i.e. lipoxidation).

Further experimental studies on modern feathers and comparisons with the fossil record are required to explain why keratin is not preserved in *Anchiornis* feathers although melanin has been detected and melanosomes and moulds have been observed.

CONCLUSION

The methods used in this study provide new and complementary information on how the plumage of *Anchiornis huxleyi* (YFGP-T5199) is preserved. SEM and EDS reveal that fossil feathers are preserved in a fine-grained material constituted of K-rich phyllosilicates, illite and interstratified illite/smectite. PIXE analyses show that both light (C, N, O) and heavy (S, Na, Ca etc.) elements are present in the fossil samples, even at very low concentrations. The presence of iron oxide pseudomorphs after pyrite probably indicates a reduced depositional environment for *Anchiornis*. Carbon is the dominant element in the fossil feathers, which are also enriched in sulphur with respect to the 'host' sediment. EBS mapping of the interior of the samples revealed a decrease in carbon concentration with depth. Our analysis therefore shows that the fossil feathers are preserved in the uppermost part of the sample, as a thin (*c.* 3 μm -thick) S-bearing carbonaceous layer. High-resolution imaging of the feather microstructure revealed the presence of elongated microbodies (650–950 nm), probably corresponding to eumelanosomes. Molecular characterization of the organic matter in the 'host' sediment, fossil feathers and modern feathers by ^{13}C NMR, micro-ATR FTIR and Py-GC-MS shows that the fossil does not display the complex amino-acid signature typical for keratin, the main constituent of modern feathers. Although the organic matter of the fossil feathers and their 'host' sediment are both dominated by aliphatic moieties, they exhibit substantial differences (distribution pattern of series, occurrence of components specific to the feathers) suggesting that the organic matter of the fossil feathers is derived, at least partially, from original constituents of the feathers.

Altogether, these results show that the fossil feathers can be described as compression fossils, as described in Schweitzer (2011, p. 192). The finely grained (clay-rich) host sediment contributed to the morphological preservation of *Anchiornis* soft tissues. As stressed by Schweitzer (2011, p. 192), the very fine grain size of the sediments might have prevented the degradation of soft tissues by microbes, and subsequent loss of degraded organic matter in the environment before and during diagenesis. However, the lack of protein-derived moieties in the fossil organic matter shows that the latter has been significantly altered during diagenesis. The excellent morphological preservation of the fossil soft tissue is not associated here with a high preservation level of organic matter. Hence, the fossil feathers have probably undergone a complex diagenetic history including several steps affecting differentially their morphology and chemistry. *In situ* polymerization of lipids into more stable aliphatic compounds during early diagenesis was probably the main process responsible for organic matter preservation in the fossil

feathers. Additionally, sulphur was probably involved in several steps of the fossil preservation although no natural sulphurization took place.

Our results are therefore unique by combining different analytical techniques on Jurassic fossil feathers. This integrative multidisciplinary study appears as a powerful approach to decipher morphological, mineralogical, structural and chemical features of fossil soft tissues and their fossilization processes.

This study provides new insights into the taphonomy of labile compounds, suggesting that keratin, unlike the pigment melanin, is not present in the feathers of *Anchiornis huxleyi* (YFGP-T5199). Our results therefore question the preservation potential of keratin (and melanin) in anoxic conditions. Further analyses of fossil feathers of different ages, showing different modes of preservation and deposited in various environmental settings are required to better understand the preservation potential of melanin and keratin.

Finally, we used here for the first time on a Jurassic fossil ion beam analysis (IBA), a non-destructive analytical technique providing an in-depth profiling of C to U elements. Further developments of this technique to palaeontological samples might help at identifying the precise location of fossil soft tissues within the sediment and then characterizing metal elements that are directly associated with the fossilized tissues.

Acknowledgements. This work was made possible through a FRIA grant provided to AC by the 'Fonds National pour la Recherche Scientifique' (FRS-FNRS). Gaëtan Rochez (UNamur) is thanked for his technical support in XRD analyses. Julien Cillis and Thierry Leduc (RBINS) are thanked for their grateful help in SEM image acquisition and EDS analyses. Maria McNamara (UCC) is warmly thanked for her advice and comments. We also thank Dr Geoffrey Grime of the Ion Beam Centre, University of Surrey, UK, for his valuable advice regarding the PIXE measurements. AC is currently funded by the Irish Research Council (GOIPD/2018/768). The authors wish to thank anonymous reviewers whose comments greatly helped to improve this manuscript.

DATA ARCHIVING STATEMENT

Additional data for this study are available in the Dryad Digital Repository: <https://doi.org/10.5061/dryad.1281jm4>

Editor. Robert Sansom

REFERENCES

- ADHYARU, B. B., AKHMEDOV, N. D., KATRITZKY, A. R. and BOWERS, C. R. 2003. Solid-state cross-polarization magic angle spinning ^{13}C and ^{15}N NMR characterization

- of Sepia melanin, Sepia melanin free acid and Human hair melanin in comparison with several model compounds. *Magnetic Resonance in Chemistry*, **41**, 466–474.
- ALLISON, P. A. and BRIGGS, D. E. G. 1993. Exceptional fossil record: distribution of soft-tissue preservation through the Phanerozoic. *Geology*, **21**, 527–532.
- ANDERSEN, F. A. and BREČEVIĆ, L. 1991. Infrared spectra of amorphous and crystalline calcium carbonate. *Acta Chemica Scandinavica*, **45** (10), 1018–1024.
- ARAI, K. M., TAKAHASHI, R., YOKOTE, Y. and AKAHANE, K. 1983. Amino acid sequence of feather keratin from fowl. *The FEBS Journal*, **132** (3), 501–507.
- 1986. The primary structure of feather keratins from duck (*Anas platyrhynchos*) and pigeon (*Columba livia*). *Biochimica et Biophysica Acta (BBA) - Protein Structure & Molecular Enzymology*, **873** (1), 6–12.
- BAAS, M., BRIGGS, D., VAN HEEMST, J., KEAR, A. and DE LEEUW, J. 1995. Selective preservation of chitin during the decay of shrimp. *Geochimica et Cosmochimica Acta*, **59** (5), 945–951.
- BARDEN, H. E., WOGELIUS, R. A., LI, D., MANNING, P. L., EDWARDS, N. P. and VAN DONGEN, B. E. 2011. Morphological and geochemical evidence of eumelanin preservation in the feathers of the Early Cretaceous bird, *Gansus yumenensis*. *PLoS One*, **6** (10), e25494.
- BERGMANN, U., EDWARDS, N. P., EGERTON, V. M., MANNING, P. L., PERRY, S., VAN VEELEN, A., WOGELIUS, R. A. and VAN DONGEN, B. E. 2015. Bacteria or melanosomes? A geochemical analysis of microbodies on a tadpole from the Oligocene Enspel Formation of Germany. *Palaeobiodiversity & Palaeoenvironments*, **95** (1), 33–45.
- BARONE, J. R., SCHMIDT, W. F. and LIEBNER, C. F. E. 2005. Thermally processed keratin films. *Journal of Applied Polymer Science*, **97**, 1644–1651.
- BARTHEL, K. 1964. Zur Entstehung der Solnhofen Plattenkalke (unteres Untertithon). *Mitteilungen der Bayerischen Staatssammlung für Paläontologie und Historische Geologie*, **4**, 37–69.
- BASIUK, V. A. and NAVARRO-GONZÁLEZ, R. 1997. Identification of hexahydroimidazo [1, 2-a] pyrazine-3, 6-diones and hexahydroimidazo [1, 2-a] imidazo [1, 2-d] pyrazine-3, 8-diones, unusual products of silica-catalyzed amino acid thermal condensation and products of their thermal decomposition using coupled high-performance liquid chromatography–particle beam mass spectrometry and gas chromatography–Fourier transform infrared spectroscopy–mass spectrometry. *Journal of Chromatography A*, **776** (2), 255–273.
- BECK, L. 2014. Recent trends in IBA for cultural heritage studies. *Nuclear Instruments & Methods in Physics Research B*, **332**, 439–444.
- BENDIT, E. G. 1966. Infrared absorption spectrum of keratin. I. Spectra of α -, β -, and supercontracted keratin. *Biopolymers*, **4**, 539–559.
- BENTON, M. J., ZHONGHE, Z., ORR, P. J., FUCHENG, Z. and KEARNS, S. L. 2008. The remarkable fossils from the Early Cretaceous Jehol Biota of China and how they have changed our knowledge of Mesozoic life. *Proceedings of the Geologists' Association*, **119**, 209–229.
- BLANCO, A., BOLAÑOS-SÁNCHEZ, U., LIZÁRRAGA-MENDIOLA, L., HERNÁNDEZ-ÁVILA, J., ÁNGELES-TRIGUEROS, S., AMBROCIO, P. and GONZÁLEZ-SANDOVAL, M. 2013. Microscopic evidences of replacement of iron sulfide by iron oxide in macro fossils: a useful tool for the search of life in Mars? *Lunar & Planetary Science Conference*, **44**, 2956.
- BORTOLOTTI, G. R. 2010. Flaws and pitfalls in the chemical analysis of feathers: bad news–good news for avian chemocology and toxicology. *Ecological Applications*, **20** (6), 1766–1774.
- BREBU, M. and SPIRIDON, I. 2011. Thermal degradation of keratin waste. *Journal of Analytical & Applied Pyrolysis*, **91** (2), 288–295.
- BRIGGS, D. E. G., BOTTRELL, S. H. and RAISWELL, R. 1991. Pyritization of soft-bodied fossils: Beecher's trilobite bed, Upper Ordovician, New York State. *Geology*, **19** (12), 1221–1224.
- KEAR, A., MARTILL, D. and WILBY, P. 1993. Phosphatization of soft-tissue in experiments and fossils. *Journal of the Geological Society*, **150** (6), 1035–1038.
- BUTTERFIELD, N. J., BALTHASAR, U. and WILSON, L. A. 2007. Fossil diagenesis in the Burgess Shale. *Palaeontology*, **50** (3), 537–543.
- CAMPBELL, J., BOYD, N., GRASSI, N., BONNICK, P. and MAXWELL, J. 2010. The Guelph PIXE software package IV. *Nuclear Instruments & Methods in Physics Research B*, **268** (20), 3356–3363.
- CANFIELD, D. E. 1989. Reactive iron in marine sediments. *Geochimica et Cosmochimica Acta*, **53** (3), 619–632.
- CARNEY, R. M., VINTHER, J., SHAWKEY, M. D., D'ALBA, L. and ACKERMANN, J. 2012. New evidence on the colour and nature of the isolated *Archaeopteryx* feather. *Nature Communications*, **3** (1), 1–6.
- CENTENO, S. A. and SHAMIR, J. 2008. Surface enhanced Raman scattering (SERS) and FTIR characterization of the sepia melanin pigment used in works of art. *Journal of Molecular Structure*, **873** (1–3), 149–159.
- CESARINI, J. P. 1996. Melanins and their possible roles through biological evolution. *Advances in Space Research*, **18** (12), 35–40.
- CHANG, S. C., ZHANG, H., RENNE, P. R. and FANG, Y. 2009. High-precision $^{40}\text{Ar}/^{39}\text{Ar}$ age constraints on the basal Lanqi Formation and its implications for the origin of angiosperm plants. *Earth & Planetary Science Letters*, **279** (3), 212–221.
- CHOI, S. S., KIM, M. C. and KIM, Y. K. 2013. Formation of methoxybenzenes from cellulose in the presence of tetramethylammonium hydroxide by pyrolysis. *Bulletin of the Korean Chemical Society*, **34** (2), 649–652.
- CHRISTIANSEN, P. and BONDE, N. 2004. Body plumage in *Archaeopteryx*: a review and new evidence from the Berlin specimen. *Comptes Rendus Palevol*, **3** (2), 99–118.
- CHU, Z., HE, H., RAMEZANI, J., BOWRING, S. A., HU, D., ZHANG, L., ZHENG, S., WANG, X., ZHOU, Z. and DENG, C. 2016. High-precision U–Pb geochronology of the Jurassic Yanliao Biota from Jianchang (western

- Liaoning Province, China): age constraints on the rise of feathered dinosaurs and eutherian mammals. *Geochemistry, Geophysics, Geosystems*, **17** (10), 3983–3992.
- CINCOTTA, A., PESTCHEVITSKAYA, E. B., SINITSKA, S. M., MARKEVICH, V. S., DEBAILLE, V., RESHETOVA, S. A., MASHCHUK, I. M., FROLOV, A. O., GERDES, A., YANS, J. and GODEFROIT, P. 2019. The rise of feathered dinosaurs: *Kulindadromeus zabaikalicus*, the oldest dinosaur with 'feather-like' structures. *PeerJ*, **7**, e6239.
- NGUYEN TU, T. T., COLAUX, J. L., TERWAGNE, G., DERENNE, S., GODEFROIT, P., CARLEER, R., ANQUETIL, C. and YANS, J. 2020. Data from: Chemical preservation of tail feathers from *Anchiornis huxleyi*, a theropod dinosaur from the Tiaojishan Formation (Upper Jurassic, China). *Dryad Digital Repository*. <https://doi.org/10.5061/dryad.1281jm4>
- COLLEARY, C., DOLOCAN, A., GARDNER, J., SINGH, S., WUTTKE, M., RABENSTEIN, R., HABERSETZER, J., SCHAAAL, S., FESEHA, M. and CLEMENS, M. 2015. Chemical, experimental, and morphological evidence for diagenetically altered melanin in exceptionally preserved fossils. *Proceedings of the National Academy of Sciences*, **112** (41), 12592–12597.
- DUFF, G. A., ROBERTS, J. E. and FOSTER, N. 1988. Analysis of the structure of synthetic and natural melanins by solid-phase NMR. *Biochemistry*, **27**, 7112–7116.
- DUTTA, S., HARTKOPF-FRÖDER, C., MANN, U., WILKES, H., BROCKE, R. and BERTRAM, N. 2010. Macromolecular composition of Palaeozoic scolecodonts: insights into the molecular taphonomy of zoomorphs. *Lethaia*, **43** (3), 334–343.
- EDWARDS, N. P., VAN VEELLEN, A., ANNÉ, J., MANNING, P. L., BERGMANN, U., SELLERS, W. I., EGER-TON, V. M., SOKARAS, D., ALONSO-MORI, R., WAKAMATSU, K. and ITO, S. 2016. Elemental characterisation of melanin in feathers via synchrotron X-ray imaging and absorption spectroscopy. *Scientific Reports*, **6**, 34002.
- FARRELL, Ú. C., BRIGGS, D. E. G., HAMMARLUND, E. U., SPERLING, E. A. and GAINES, R. R. 2013. Paleoredox and pyritization of soft-bodied fossils in the Ordovician Frankfort Shale of New York. *American Journal of Science*, **313** (5), 452–489.
- FRASER, R. D. B. and MACRAE, T. P. 2012. *Conformation in fibrous proteins and related synthetic polypeptides*. Academic Press, 648 pp.
- and PARRY, D. A. D. 1996. The molecular structure of reptilian keratin. *International Journal of Biological Macromolecules*, **19** (3), 207–211.
- GABBOTT, S., NORRY, M., ALDRIDGE, R. and THERON, J. 2001. Preservation of fossils in clay minerals; a unique example from the Upper Ordovician Soom Shale, South Africa. *Proceedings of the Yorkshire Geological Society*, **53** (3), 237–244.
- GALLOIS, N., TEMPLIER, J. and DERENNE, S. 2007. Pyrolysis-gas chromatography-mass spectrometry of the 20 protein amino acids in the presence of TMAH. *Journal of Analytical & Applied Pyrolysis*, **80**, 216–230.
- GIRALDO, L. and MORENO-PIRAJÁN, J. C. 2013. Exploring the use of rachis of chicken feathers for hydrogen storage. *Journal of Analytical & Applied Pyrolysis*, **104**, 243–248.
- GODEFROIT, P., CAU, A., DONG-YU, H., ESCUILLIÉ, F., WENHAO, W. and DYKE, G. 2013. A Jurassic avialan dinosaur from China resolves the early phylogenetic history of birds. *Nature*, **498** (7454), 359–362.
- SINITSKA, S. M., DHOUILLY, D., BOLOTSKY, Y. L., SIZOV, A. V., MCNAMARA, M. E., BENTON, M. J. and SPAGNA, P. 2014. A Jurassic ornithischian dinosaur from Siberia with both feathers and scales. *Science*, **345** (6), 451–455.
- CINCOTTA, A., MCNAMARA, M. E., RESHETOVA, S. A. and DHOUILLY, D. 2020. Integumentary structures in *Kulindadromeus zabaikalicus*, a Basal Neornithischian Dinosaur from the Jurassic of Siberia. 47–65. In FOTH, C. and RAUHUT, O. W. M. (eds). *The evolution of feathers*. Springer.
- GRADSTEIN, F. M., OGG, J. G., SCHMITZ, M. and OGG, G. 2012. *The geologic time scale 2012*. Elsevier.
- GREGG, K. and ROGERS, G. E. 1986. Feather keratin: composition, structure and biogenesis. 666–694. In BEREITERHAHN, J., MATOLSKY, A. G. and RICHARDS, K. S. (eds). *Biology of the integument*. Springer.
- GUPTA, N. S., MICHELS, R., BRIGGS, D. E., COLLINSON, M. E., EVERSHED, R. P. and PANCOST, R. D. 2007. Experimental evidence for the formation of geomacromolecules from plant leaf lipids. *Organic Geochemistry*, **38** (1), 28–36.
- CAMBRA-MOO, O., BRIGGS, D. E., LOVE, G. D., FREGENAL-MARTINEZ, M. A. and SUMMONS, R. E. 2008. Molecular taphonomy of macrofossils from the Cretaceous Las Hoyas Formation, Spain. *Cretaceous Research*, **29** (1), 1–8.
- GURBICH, A. 2016. SigmaCalc recent development and present status of the evaluated cross-sections for IBA. *Nuclear Instruments & Methods in Physics Research B*, **371**, 27–32.
- HARMS, F. 2002. Steine erzählen Geschichte (n): Ursache für die Entstehung des Messel-Sees gefunden. *Natur und Museum*, **132** (1), 1–4.
- HARRAP, B. S. and WOODS, E. F. 1964. Soluble derivatives of feather keratin: 1. Isolation, fractionation and amino acid composition. *Biochemical Journal*, **92** (1), 8.
- 1967. Species differences in the proteins of feathers. *Comparative Biochemistry & Physiology*, **20** (2), 449–460.
- HEIMHOFER, R. and MARTILL, D. 2007. The sedimentology and depositional environment of the Crato Formation. 44–62. In MARTILL, D. M., BECHLY, G. and LOVERIDGE, R. F. (eds). *The Crato fossil beds of Brazil: Window into an ancient world*. Cambridge University Press.
- HENDRICKER, A. D. and VOORHEES, K. J. 1996. An investigation into the Curie-point pyrolysis-mass spectrometry of glycyl dipeptides. *Journal of Analytical & Applied Pyrolysis*, **36** (1), 51–70.
- HU, D., HOUL, L., ZHANG, L. and XU, X. 2009. A pre-*Archaeopteryx* troodontid theropod from China with long feathers on the metatarsus. *Nature*, **461** (7264), 640.

- CLARKE, J. A., ELIASON, C. M., QIU, R., LI, Q., SHAWKEY, M. D., ZHAO, C., D'ALBA, L., JIANG, J. and XU, X. 2018. A bony-crested Jurassic dinosaur with evidence of iridescent plumage highlights complexity in early paravian evolution. *Nature Communications*, **9** (1), 1–12.
- ITO, S. and NICOL, J. C. 1974. Isolation of oligomers of 5, 6-dihydroxyindole-2-carboxylic acid from the eye of the catfish. *Biochemical Journal*, **143** (1), 207–217.
- JAIN, D., STARK, A. Y., NIEWIAROWSKI, P. H., MIYOSHI, T. and DHINOJWALA, A. 2015. NMR spectroscopy reveals the presence and association of lipids and keratin in adhesive gecko setae. *Scientific Reports*, **5**, 9594.
- JEYNES, C. and COLAUX, J. L. 2016. Thin film depth profiling by ion beam analysis. *Analyst*, **141** (21), 5944–5985.
- BARRADAS, N., MARRIOTT, P., BOUDREAU, G., JENKIN, M., WENDLER, E. and WEBB, R. 2003. Elemental thin film depth profiles by ion beam analysis using simulated annealing—a new tool. *Journal of Physics D*, **36** (70), R97.
- JI, Q. and JI, S. 1996. On the Discovery of the earliest fossil bird in China (*Sinosauropteryx* gen. nov.) and the origin of birds. *Chinese Geology*, **233**, 6.
- KAYE, T. G., GAUGLER, G. and SAWLOWICZ, Z. 2008. Dinosaurian soft tissues interpreted as bacterial biofilms. *PLoS One*, **3** (7), e2808.
- KELLNER, A. W. A. and DE ALMEIDA CAMPOS, D. 2002. The function of the cranial crest and jaws of a unique pterosaur from the Early Cretaceous of Brazil. *Science*, **297**, 389–392.
- KELLNER, A. W., WANG, X., TISCHLINGER, H., DE ALMEIDA CAMPOS, D., HONE, D. W. and MENG, X. 2010. The soft tissue of *Jeholopterus* (Pterosauria, Anurognathidae, Batrachognathinae) and the structure of the pterosaur wing membrane. *Proceedings of the Royal Society B*, **277** (1679), 321–329.
- KING, J. R. and MURPHY, M. E. 1987. Amino acid composition of the calamus, rachis, and barbs of white-crowned sparrow feathers. *The Condor*, **89** (2), 436–439.
- KIROS, A., GHOLAP, A. V. and GIGANTE, G. E. 2013. Fourier transform infrared spectroscopic characterization of clay minerals from rocks of Lalibela churches, Ethiopia. *International Journal of Physical Sciences*, **8** (3), 109–119.
- KRICHELDORF, H. R. and MÜLLER, D. 1984. Secondary structure of peptides 16th. Characterization of proteins by means of ¹³C NMR CP/MAS spectroscopy. *Colloid & Polymer Science*, **262**, 856–861.
- KRÖNER, S. U., DOMENECH CARBO, M. and MAS BARBERÀ, X. 2010. Hydraulic lime mortar in the ambit of stone restoration: evaluation of applicability. *Arché*, **4–5**, 181–188.
- LENG, Q. and YANG, H. 2003. Pyrite framboids associated with the Mesozoic Jehol biota in northeastern China: implications for microenvironment during early fossilization. *Progress in Natural Science*, **13** (3), 206–212.
- LI, Q., GAO, K.-Q., VINTHER, J., SHAWKEY, M. D., CLARKE, J. A., D'ALBA, L., MENG, Q., BRIGGS, D. E. G. and PRUM, R. O. 2010. Plumage color patterns of an extinct dinosaur. *Science*, **327**, 1369–1372.
- — — MENG, Q., CLARKE, J. A., SHAWKEY, M. D., D'ALBA, L., PEI, R., ELLISON, M., NORELL, M. A. and VINTHER, J. 2012. Reconstruction of *Microraptor* and the evolution of iridescent plumage. *Science*, **335**, 1215.
- LINDGREN, J., UVDAL, P., SJÖVALL, P., NILSSON, D. E., ENGDAHL, A., SCHULTZ, B. P. and THIEL, V. 2012. Molecular preservation of the pigment melanin in fossil melanosomes. *Nature Communications*, **3** (1), 1–7.
- SJÖVALL, P., CARNEY, R. M., CINCOTTA, A., UVDAL, P., HUTCHESON, S. W., GUSTAFSSON, O., LEFÈVRE, U., ESCUILLIER, F., HEIMDAL, J., ENGDAHL, A., GREN, J. A., KEAR, B. P., WAKAMATSU, K., YANS, J. and GODEFROIT, P. 2015. Molecular composition and ultrastructure of Jurassic paravian feathers. *Scientific Reports*, **5**, 13520.
- UVDAL, P., SJÖVALL, P., NILSSON, D. E., ENGDAHL, A., SCHULTZ, B. P. and THIEL, V. 2012. Molecular preservation of the pigment melanin in fossil melanosomes. *Nature Communications*, **3** (1), 1–7.
- LIU, Y. Q., KUANG, H. W., JIANG, X. J., PENG, N., XU, H. and SUN, H. Y. 2012. Timing of the earliest known feathered dinosaurs and transitional pterosaurs older than the Jehol Biota. *Palaeogeography, Palaeoclimatology, Palaeoecology*, **323–325**, 1–12.
- LUCAS, A. M. and STETTENHEIM, P. R. 1972. *Avian anatomy: integuments*. US Department of Agriculture & Michigan Agricultural Experiment Station, Washington, DC.
- MANNING, P. L., MORRIS, P. M., McMAHON, A., JONES, E., GIZE, A., MACQUAKER, J. H., WOLFF, G., THOMPSON, A., MARSHALL, J. and TAYLOR, K. G.. 2009. Mineralized soft-tissue structure and chemistry in a mummified hadrosaur from the Hell Creek Formation, North Dakota (USA). *Proceedings of the Royal Society B*, **276** (1672), 3429–3437.
- EDWARDS, N. P., WOGELIUS, R. A., BERGMANN, U., BARDEN, H. E., LARSON, P. L., SCHWARZ-WINGS, D., EGERTON, V. M., SOKARAS, D. and MORI, R. A.. 2013. Synchrotron-based chemical imaging reveals plumage patterns in a 150 million year old early bird. *Journal of Analytical Atomic Spectrometry*, **28** (7), 1024–1030.
- MARTILL, D. M. and HEIMHOFER, U. 2007. Stratigraphy of the Crato Formation. 25–43. In MARTILL, D. M., BECHLY, G. and LOVERIDGE, R. F. (eds). *The Crato fossil beds of Brazil: Window into an ancient world*. Cambridge University Press.
- MARTIN, D., BRIGGS, D. E. and PARKES, R. J. 2004. Experimental attachment of sediment particles to invertebrate eggs and the preservation of soft-bodied fossils. *Journal of the Geological Society*, **161** (5), 735–738.
- MAYR, G., PETERS, D. S., PLODOWSKI, G. and VOGEL, O. 2002. Bristle-like integumentary structures at the tail of the horned dinosaur *Psittacosaurus*. *Naturwissenschaften*, **89**, 361–365.
- McNAMARA, M. E., VAN DONGEN, B. E., LOCKYER, N. P., BULL, I. D. and ORR, P. J. 2016. Fossilization of melanosomes via sulfurization. *Palaeontology*, **59** (3), 1–14.

- MOLDOVEANU, S. C. 2009. *Pyrolysis of organic molecules: Applications to health and environmental issues*. Techniques & instrumentation in analytical chemistry, **28**. Elsevier, 723 pp.
- MOYER, A. E., ZHENG, W. and SCHWEITZER, M. H. 2016. Keratin durability has implications for the fossil record: results from a 10 year feather degradation experiment. *PLoS One*, **11** (7), e0157699.
- MURPHY, M. E., KING, J. R., TARUSCIO, T. G. and GEUPEL, G. R. 1990. Amino acid composition of feather barbs and rachises in three species of pygoscelid penguins: nutritional implications. *The Condor*, **92** (4), 913–921.
- NAN, P., YONGQING, L., HONGWEI, K., XIAOJUN, J. and HUAN, X. 2012. Stratigraphy and geochronology of vertebrate fossil-bearing Jurassic strata from Linglongta, Jianchang County, Western Liaoning, Northeastern China. *Acta Geologica Sinica (English Edition)*, **86** (6), 1326–1339.
- NORDSTROM, D. K. 1982. Aqueous pyrite oxidation and the consequent formation of secondary iron minerals. 37–56. In KITTRICK, J. A., FANNING, D. S. and HOSSNER, L. R. (eds). *Acid sulfate weathering*. Soil Science Society of America Special Publication, **10**.
- O'DONNELL, I. and INGLIS, A. 1974. Amino acid sequence of a feather keratin from Silver Gull (*Larus novae-hollandiae*) and comparison with one from Emu (*Dromaius novae-hollandiae*). *Australian Journal of Biological Sciences*, **27** (4), 369–382.
- O'REILLY, S., SUMMONS, R., MAYR, G. and VINTHER, J. 2017. Preservation of uropygial gland lipids in a 48-million-year-old bird. *Proceedings of the Royal Society B*, **284**, 20071050.
- PAN, Y., SHA, J., ZHOU, Z. and FÜRSICH, F. T. 2013. The Jehol Biota: definition and distribution of exceptionally preserved relicts of a continental Early Cretaceous ecosystem. *Cretaceous Research*, **44**, 30–38.
- ZHENG, W., MOYER, A. E., O'CONNOR, J. K., WANG, M., ZHENG, X., WANG, X., SCHROETER, E. R., ZHOU, Z. and SCHWEITZER, M. H. 2016. Molecular evidence of keratin and melanosomes in feathers of the Early Cretaceous bird *Eoconfuciusornis*. *Proceedings of the National Academy of Sciences*, **113** (49), E7900–E7907.
- RATCLIFF, M. A. Jr, MEDLEY, E. E. and SIMMONDS, P. G. 1974. Pyrolysis of amino acids. Mechanistic considerations. *The Journal of Organic Chemistry*, **39** (11), 1481–1490.
- RAUHUT, O. W., FOTH, C., TISCHLINGER, H. and NORELL, M. A. 2012. Exceptionally preserved juvenile megalosauroid theropod dinosaur with filamentous integument from the Late Jurassic of Germany. *Proceedings of the National Academy of Sciences*, **109** (29), 11746–11751.
- RILEY, P. A. 1997. Melanin. *The International Journal of Biochemistry & Cell Biology*, **29** (11), 1235–1239.
- SAITTA, E. T., ROGERS, C., BROOKER, R. A., ABBOTT, G. D., KUMAR, S., O'REILLY, S. S., DONOHUE, P., DUTTA, S., SUMMONS, R. E. and VINTHER, J. 2017. Low fossilization potential of keratin protein revealed by experimental taphonomy. *Palaeontology*, **60** (4), 547–556.
- SARAVANAN, K. and DHURAI, B. 2012. Exploration on amino acid content and morphological structure in chicken feather fiber. *Journal of Textile and Apparel, Technology & Management*, **7** (3), 1–6.
- SCHWEITZER, M. H. 2011. Soft tissue preservation in terrestrial Mesozoic vertebrates. *Annual Review of Earth & Planetary Sciences*, **39**, 187–216.
- WATT, J. A., AVCI, R., FORSTER, C. A., KRAUSE, D. W., KNAPP, L., ROGERS, R. R., BEECH, I. and MARSHALL, M. 1999. Keratin immunoreactivity in the Late Cretaceous bird *Rahonavis ostromi*. *Journal of Vertebrate Paleontology*, **19** (4), 712–722.
- SEITZ, L. M. and RAM, M. 2000. Volatile methoxybenzene compounds in grains with off-odors. *Journal of Agricultural & Food Chemistry*, **48** (9), 4279–4289.
- SHARMA, S., GUPTA, A., KUMAR, A., KEE, C. G., KAMYAB, H. and SAUFI, S. M. 2018. An efficient conversion of waste feather keratin into ecofriendly bioplastic film. *Clean Technologies & Environmental Policy*, **20** (10), 2157–2167.
- SIMMONDS, P., MEDLEY, E., RATCLIFF, M. and SHULMAN, G. 1972. Thermal decomposition of aliphatic monoaminomonocarboxylic acids. *Analytical Chemistry*, **44** (12), 2060–2066.
- SINNINGHE-DAMSTÉ, J. S. and DE LEEUW, J. W. 1990. Analysis, structure and geochemical significance of organically-bound sulphur in the geosphere: state of the art and future research. *Organic Geochemistry*, **16** (4–6), 1077–1101.
- IRENE, W., RIJPSMA, C., DE LEEUW, J. W. and SCHENCK, P. 1988. Origin of organic sulphur compounds and sulphur-containing high molecular weight substances in sediments and immature crude oils. *Organic Geochemistry*, **13** (4–6), 593–606.
- EGLINTON, T. I., DE LEEUW, J. W. and SCHENCK, P. 1989. Organic sulphur in macromolecular sedimentary organic matter: I. Structure and origin of sulphur-containing moieties in kerogen, asphaltene and coal as revealed by flash pyrolysis. *Geochimica et Cosmochimica Acta*, **53** (4), 873–889.
- SLATER, T. S., MCNAMARA, M. E., ORR, P. J., FOLEY, T. B., ITO, S. and WAKAMATSU, K. 2020. Taphonomic experiments resolve controls on the preservation of melanosomes and keratinous tissues in feathers. *Palaeontology*, **63** (1), 103–115.
- STANKIEWICZ, B., SCOTT, A., COLLINSON, M. E., FINCH, P., MÖSLE, B., BRIGGS, D. and EVERSLED, R. 1998. Molecular taphonomy of arthropod and plant cuticles from the Carboniferous of North America: implications for the origin of kerogen. *Journal of the Geological Society*, **155** (3), 453–462.
- BRIGGS, D. E. G., MICHELS, R., COLLINSON, M., FLANNERY, M. and EVERSLED, R. 2000. Alternative origin of aliphatic polymer in kerogen. *Geology*, **28** (6), 559–562.
- STAROŃ, P., BANACH, M. and KOWALSKI, Z. 2011. Keratyna: źródła, właściwości, zastosowanie. *Chemik*, **65** (10), 1019–1026.
- STĘPIEŃ, K., DZIERŻĘGA-ŁĘCZNA, A., KURKIEWICZ, S. and TAM, I. 2009. Melanin from epidermal human melanocytes: study by pyrolytic GC/MS. *Journal of the American Society for Mass Spectrometry*, **20** (3), 464–468.
- SULLIVAN, C., WANG, Y., HONE, D. W., WANG, Y., XU, X. and ZHANG, F. 2014. The vertebrates of the

- Jurassic Daohugou Biota of northeastern China. *Journal of Vertebrate Paleontology*, **34** (2), 243–280.
- TEGELAAR, E. W., DE LEEUW, J. W., DERENNE, S. and LARGEAU, C. 1989. A reappraisal of kerogen formation. *Geochimica et Cosmochimica Acta*, **53** (11), 3103–3106.
- TEMPLIER, J., GALLOIS, N. and DERENNE, S. 2013. Analytical TMAH pyrolysis of dipeptides: formation of new complex cyclic compounds related to the presence of the peptide bond. *Journal of Analytical & Applied Pyrolysis*, **104**, 684–694.
- TESFAYE, T., SITHOLE, B., RAMJUGERNATH, D. and CHUNILALL, V. 2017. Valorisation of chicken feathers: characterisation of chemical properties. *Waste Management*, **68**, 626–635.
- WANG, Y. X. and CAO, X. J. 2012. Extracting keratin from chicken feathers by using a hydrophobic ionic liquid. *Process Biochemistry*, **47**, 896–899.
- WANG, B., ZHAO, F., ZHANG, H., FANG, Y. and ZHENG, D. 2012. Widespread pyritization of insects in the Early Cretaceous Jehol Biota. *Palaio*, **27** (10), 708–712.
- WANG, M., O'CONNOR, J. K., XU, X. and ZHOU, Z. 2019. A new Jurassic scansoriopterygid and the loss of membranous wings in theropod dinosaurs. *Nature*, **569** (7755), 256–259.
- WERNE, J. P., HOLLANDER, D. J., BEHRENS, A., SCHAEFFER, P., ALBRECHT, P. and SINNINGHE DAMSTÉ, J. S. 2000. Timing of early diagenetic sulfurization of organic matter: a precursor-product relationship in Holocene sediments of the anoxic Cariaco Basin, Venezuela. *Geochimica et Cosmochimica Acta*, **64** (10), 1741–1751.
- WIEMANN, J., FABBRI, M., YANG, T. R., STEIN, K., SANDER, P. M., NORELL, M. A. and BRIGGS, D. E. 2018. Fossilization transforms vertebrate hard tissue proteins into N-heterocyclic polymers. *Nature Communications*, **9** (1), 4741.
- WILBY, P. R., BRIGGS, D. E. G. and RIOU, B. 1996. Mineralization of soft-bodied invertebrates in a Jurassic metalliferous deposit. *Geology*, **24** (9), 847–850.
- WOGELIUS, R., MANNING, P., BARDEN, H., EDWARDS, N., WEBB, S., SELLERS, W., TAYLOR, K., LARSON, P., DODSON, P. and YOU, H. 2011. Trace metals as biomarkers for eumelanin pigment in the fossil record. *Science*, **333** (6049), 1622–1626.
- WOJCIECHOWSKA, E., ROM, M., WŁOCHOWICZ, A., WYSOCKI, M. and WEŚLUCHA-BIRCZYŃSKA, A. 2004. The use of Fourier transform-infrared (FTIR) and Raman spectroscopy (FTR) for the investigation of structural changes in wool fibre keratin after enzymatic treatment. *Journal of Molecular Structure*, **704** (1–3), 315–321.
- XING, L., MCKELLAR, R. C., XU, X., LI, G., BAI, M., PERSONS, W. S., MIYASHITA, T., BENTON, M. J., ZHANG, J. and WOLFE, A. P. 2016. A feathered dinosaur tail with primitive plumage trapped in Mid-Cretaceous amber. *Current Biology*, **26** (24), 3352–3360.
- XU, X., WANG, X. L. and WU, X. C. 1999. A dromaeosaurid dinosaur with a filamentous integument from the Yixian Formation of China. *Nature*, **401** (6750), 262–266.
- ZHAO, Q., NORELL, M., SULLIVAN, C., HONE, D., ERICKSON, G., WANG, X. L., HAN, F. L. and GUO, Y. 2009. A new feathered maniraptoran dinosaur fossil that fills a morphological gap in avian origin. *Chinese Science Bulletin*, **54** (3), 430–435.
- WANG, K., ZHANG, K., MA, Q., XING, L., SULLIVAN, C., HU, D., CHENG, S. and WANG, S. 2012. A gigantic feathered dinosaur from the Lower Cretaceous of China. *Nature*, **484** (7392), 92–95.
- ZHENG, X., SULLIVAN, C., WANG, X., XING, L., WANG, Y. X., ZHANG, X., O'CONNOR, J. K., ZHANG, F. and PAN, Y. 2015. A bizarre Jurassic maniraptoran theropod with preserved evidence of membranous wings. *Nature*, **521** (7550), 70–73.
- YANG, J. H., WU, F. Y., SHAO, J. A., WILDE, S. A., XIE, L. W. and LIU, X. M. 2006. Constraints on the timing of uplift of the Yanshan Fold and Thrust Belt, North China. *Earth & Planetary Science Letters*, **246**, 336–352.
- YOSHIMIZU, H. and ANDO, I. 1990. Conformational characterization of wool keratin and 5'-(Carboxymethyl) kerateine in the solid state by ¹³C CP/MAS NMR spectroscopy. *Macromolecules*, **23**, 2908–2912.
- YU, P., MCKINNON, J. J., CHRISTENSEN, C. R. and CHRISTENSEN, D. A. 2004. Using synchrotron-based FTIR microspectroscopy to reveal chemical features of feather protein secondary structure: comparison with other feed protein sources. *Journal of Agricultural & Food Chemistry*, **52** (24), 7353–7361.
- YUAN, H., LIU, X., LIU, Y., GAO, S. and LING, W. 2005. Geochemistry and U-Pb zircon geochronology of Late-Mesozoic lavas from Xishan, Beijing. *Science in China: Series D Earth Sciences*, **49** (1), 50–67.
- ZHANG, H., WANG, M. X. and LIU, X. M. 2008. Constraints on the upper boundary age of the Tiaojishan Formation volcanic rocks in West-Liaoning –North Hebei by LA-ICP-MS dating. *Chinese Science Bulletin*, **53** (22), 3574–3584.
- ZHANG, F., KEARNS, S. L., ORR, P. J., BENTON, M. J., ZHOU, Z., JOHNSON, D., XU, X. and WANG, X. 2010. Fossilized melanosomes and the colour of Cretaceous dinosaurs and birds. *Nature*, **463** (7284), 1075–1078.
- ZHAO, T., HU, J., HU, L. and PAN, Y. 2020. Experimental maturation of feathers: implications for interpretations of fossil feathers. *Palaio*, **35** (2), 67–76.
- ZHENG, X. T., YOU, H. L., XU, X. and DONG, Z. M. 2009. An early Cretaceous heterodontosaurid dinosaur with zfilamentous integumentary structures. *Nature*, **458**, 333–336.
- ZHOU, Z., JIN, F. and WANG, Y. 2010. Vertebrate assemblages from the Middle-Late Jurassic Yanliao Biota in northeast China. *Earth Science Frontiers*, **17**, 252–254.
- ZHU, M., BABCOCK, L. E. and STEINER, M. 2005. Fossilization modes in the Chengjiang Lagerstätte (Cambrian of China): testing the roles of organic preservation and diagenetic alteration in exceptional preservation. *Palaogeography, Palaeoclimatology, Palaeoecology*, **220**, 31–46.

APPENDIX 1

Molecular structures of compounds identified in the modern bird feathers; numbers correspond to those appearing in Table 2 and Figure 8.

